

## Accepted Manuscript

Research paper

DNA binding and cytotoxicity of two Cu(II) complexes containing a Schiff base ligand along with 1,10-phenanthroline or imidazole as a coligand

Manjuri K. Koley, Sidhali Uday Parsekar, Natarajan Duraipandy, Manikantan Syamala Kiran, Babu Varghese, Periakaruppan T. Manoharan, Aditya P. Koley

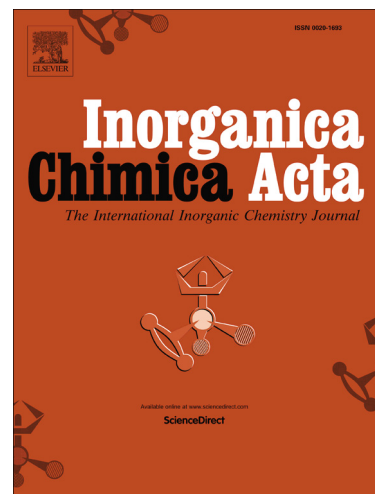
PII: S0020-1693(17)31717-6  
DOI: <https://doi.org/10.1016/j.ica.2018.04.017>  
Reference: ICA 18208

To appear in: *Inorganica Chimica Acta*

Received Date: 10 November 2017  
Revised Date: 26 February 2018  
Accepted Date: 10 April 2018

Please cite this article as: M.K. Koley, S.U. Parsekar, N. Duraipandy, M.S. Kiran, B. Varghese, P.T. Manoharan, A.P. Koley, DNA binding and cytotoxicity of two Cu(II) complexes containing a Schiff base ligand along with 1,10-phenanthroline or imidazole as a coligand, *Inorganica Chimica Acta* (2018), doi: <https://doi.org/10.1016/j.ica.2018.04.017>

This is a PDF file of an unedited manuscript that has been accepted for publication. As a service to our customers we are providing this early version of the manuscript. The manuscript will undergo copyediting, typesetting, and review of the resulting proof before it is published in its final form. Please note that during the production process errors may be discovered which could affect the content, and all legal disclaimers that apply to the journal pertain.



**DNA binding and cytotoxicity of two Cu(II) complexes containing a Schiff base ligand along with 1,10-phenanthroline or imidazole as a coligand**

Manjuri K. Koley<sup>a,\*</sup>, Sidhali Uday Parsekar<sup>a</sup>, Natarajan Duraipandy<sup>b</sup>, Manikantan Syamala Kiran<sup>b</sup>, Babu Varghese<sup>c</sup>, Periakaruppan T. Manoharan<sup>d,\*</sup> and Aditya P.

Koley<sup>e,\*</sup>

<sup>a</sup> Department of Chemical Engineering, Birla Institute of Technology and Science-Pilani, K.K. Birla Goa Campus, Goa 403726, India

<sup>b</sup> Biological Materials Laboratory, CSIR-Central Leather Research Institute, Adyar, Chennai 600 020, India

<sup>c</sup> Sophisticated Analytical Instrument Facility, Indian Institute of Technology-Madras, Chennai 600 036, India

<sup>d</sup> Department of Chemistry, Indian Institute of Technology-Madras, Chennai 600 036, India

<sup>e</sup> Department of Chemistry, Birla Institute of Technology and Science-Pilani, K.K. Birla Goa Campus, Goa 403 726, India

---

---

## Abstract

We report the synthesis, characterization and biological activities of the compounds [CuL(o-phen)] (**1**) and [CuL(Imz)] (**2**), ( $H_2L = o\text{-HOC}_6\text{H}_4\text{C(H)=NC}_6\text{H}_4\text{OH-}o$ , o-phen = 1,10-phenanthroline, and Imz = imidazole). Both the compounds **1** and **2** have been characterized by X-ray crystallography. A four-line EPR pattern originating from the interaction of the unpaired electron with the central  $^{63/65}\text{Cu}$  nucleus ( $I = 3/2$ ) with  $A_{\text{iso}}$  values of 7.3 and 8.5 mT, respectively for **1** and **2** in DMF at RT suggests their monomeric nature in solution. These compounds undergo irreversible oxidation-reduction. Biological studies show intercalative DNA binding and remarkable cell cytotoxicity as well as anticancer activity.  $\text{IC}_{50}$  values of **1** and **2** for the human lung cancer A549 cell line (0.67 and 0.59 M, respectively) and for the breast cancer MCF7 cell line (6.30 and 8.88 M, respectively) are found to be very promising. Compounds **1** and **2** appear to be more potent for the human lung cancer A549 cell line than some anticancer drugs tested for this cell line. Most importantly, **1** and **2** are found to be remarkably less toxic for the human lung embryonic normal cell line L132 as evident from the cell viabilities in presence of these two compounds.

---

*Keywords:* Cu(II) complex; EPR and electronic spectra; DNA binding; MTT assay; Cytotoxicity and anticancer activity

---

\*Corresponding authors. Email: manjuri@goa.bits-pilani.ac.in (M. K. Koley);

ptm@iitm.ac.in (P.T.)

Manoharan); koleyap@yahoo.co.in (A.P. Koley)

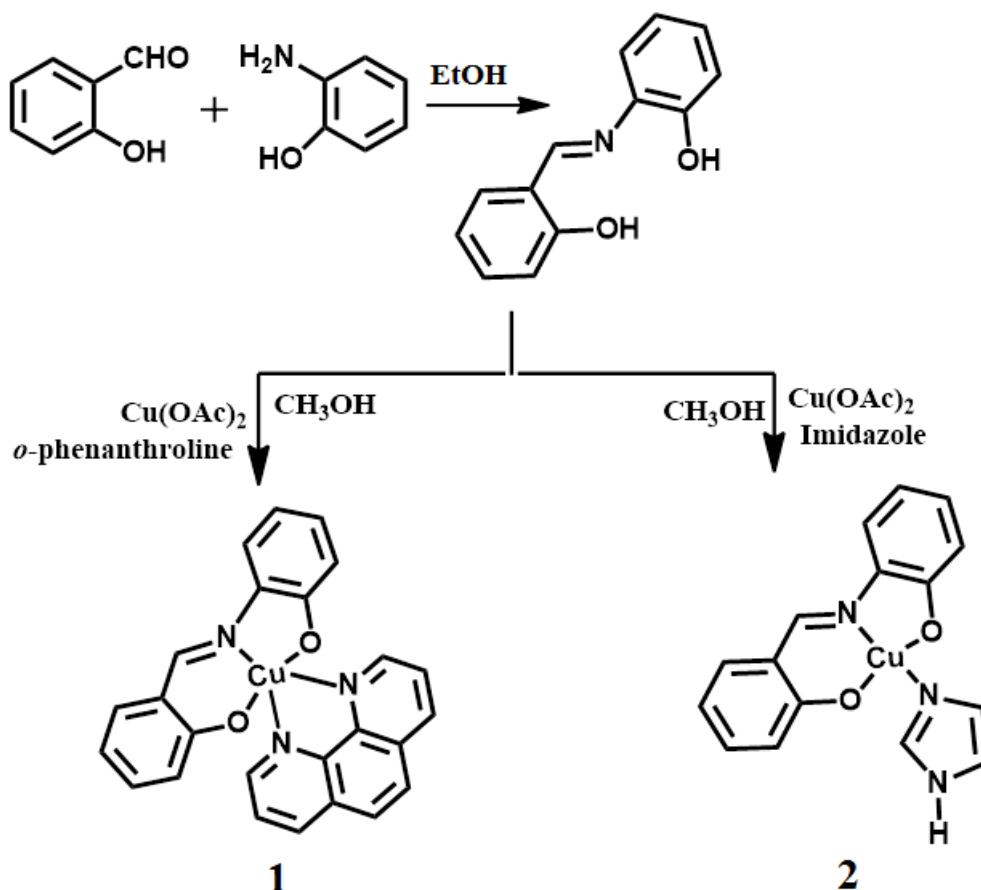
## 1. Introduction

To explore the possibility of finding new metallodrugs that may serve as anticancer agents [1-13], there have been increasing efforts in recent years to search for or design and develop metal complexes that show DNA binding property, nucleic acid cleavage activity as well as cytotoxicity. It is known that the nature of the ligand present in the metallodrugs plays a critical role in binding of the metal complex to DNA [14] which is an important target for anticancer drugs and also the metal ion may play an important role in the efficacy of the metal complex as a drug. For example, Cu(II) being a redox active metal ion may promote transformation of DNA or protein through an oxidative pathway. Very recently we have reported [15] a few Cu(II)/Zn(II) complexes with a carbohydrazone ligand along with 1,10-phenanthroline as a coligand which were found to be very promising and appeared to be more potent than some anticancer drugs tested for the human lung cancer A549 cell line and for the breast cancer MCF7 cell line as revealed from their  $IC_{50}$  values. In our continuing effort in finding metal complexes with suitable donor ligands with additional heterocyclic N-donors [15, 16], that are capable of effectively binding to DNA, we have synthesized two Cu(II) complexes, one five-coordinate and another four-coordinate, containing the Schiff base ligand N-salicylidene-*o*-aminophenol ( $H_2L = o\text{-HOC}_6\text{H}_4\text{C(H)=NC}_6\text{H}_4\text{OH-}o$ ) and 1,10-phenanthroline or imidazole as the coligand. Here, we report their spectral

(UV-visible, IR, and EPR) and electrochemical behavior as well as their biological activities such as DNA binding, cytotoxicity and anticancer activity.

## 2. Results and discussion

We have studied the reaction of  $\text{Cu}(\text{OAc})_2 \cdot \text{H}_2\text{O}$  with the Schiff base *N*-salicylidene-*o*-aminophenol (*o*- $\text{HOC}_6\text{H}_4\text{C}(\text{H})=\text{NC}_6\text{H}_4\text{OH}$ -*o*) in methanol in presence of either 1,10-phenanthroline or imidazole as the coligand to prepare the complexes **1** and **2**, respectively as shown in Scheme 1.



**Scheme 1.** Synthesis of the ligand and the complexes.

The IR spectrum of the free Schiff base ligand clearly displays the  $\nu(\text{C}=\text{N})$  band at  $1630\text{ cm}^{-1}$  [17]. This is found to be shifted to  $1608\text{ cm}^{-1}$  in the IR spectra of both the complexes (figures not shown) indicating the coordination of the imine N to the metal

ion, apart from the deprotonation and coordination of both the phenolate O. This is confirmed from the crystal structures of both **1** and **2**.

These are moderately soluble in methanol and acetonitrile but readily soluble in DMF and DMSO. The ESI-MS spectra (in the positive-ion mode) for these complexes have been recorded in CH<sub>3</sub>CN and the results are presented in Fig. S1 and Fig. S2

(Supplementary material). Complex **1** showed peaks at  $m/z$  454.30 [M]<sup>+</sup> and  $m/z$  491.30 [(M+K)-2H]<sup>+</sup> while compound **2** showed peaks at  $m/z$  343.01 [M]<sup>+</sup> and  $m/z$  344.81 [M+2H]<sup>+</sup>, respectively.

The electronic spectra of these two compounds in the visible region look very similar (Figs. S3 and S4 of the Supplementary material), but the intensities of the bands are found to be widely different. Compound **1** displays a weak broad d-d band centered around 650 nm ( $\epsilon = 144.9 \text{ M}^{-1} \text{ cm}^{-1}$ ) while compound **2** displays the weak ligand field band centered 565 nm ( $\epsilon = 45.4 \text{ M}^{-1} \text{ cm}^{-1}$ ). Apart from the weak ligand field transition [15, 16], compound **1** exhibits strong LMCT in the visible region. The charge transfer band at 434 nm ( $\epsilon = 10284 \text{ M}^{-1} \text{ cm}^{-1}$ ) for **1** containing 1,10-phenanthroline as the coligand is found to be highly intense compared to that at 440 nm ( $\epsilon = 221.9 \text{ M}^{-1} \text{ cm}^{-1}$ ) for **2** with imidazole as the coligand. Also the overall intensity for all the bands for **1** is much higher than that for **2**, showing the differences in their electronic structures.

### 2.1. Crystal structures of [CuL(o-phen)] 3.5H<sub>2</sub>O (**1**) and [CuL(Imz)] (**2**)

The structure of **1** and **2** have been determined by X-ray crystallography. Fig. 1 shows the ORTEP representation of the molecule of **1** with 40% probability ellipsoids [18].

The crystal for **1** is indexed in monoclinic system with space group C2/c and lattice

parameters  $a = 21.070(3) \text{ \AA}$ ,  $b = 20.629(3) \text{ \AA}$ ,  $c = 14.1300(16) \text{ \AA}$ ,  $\alpha = 90^\circ$ ,  $\beta = 128.704(3)^\circ$ ,  $\gamma = 90^\circ$ . The bond length and bond angles are given in Table S1 of the Supplementary material.

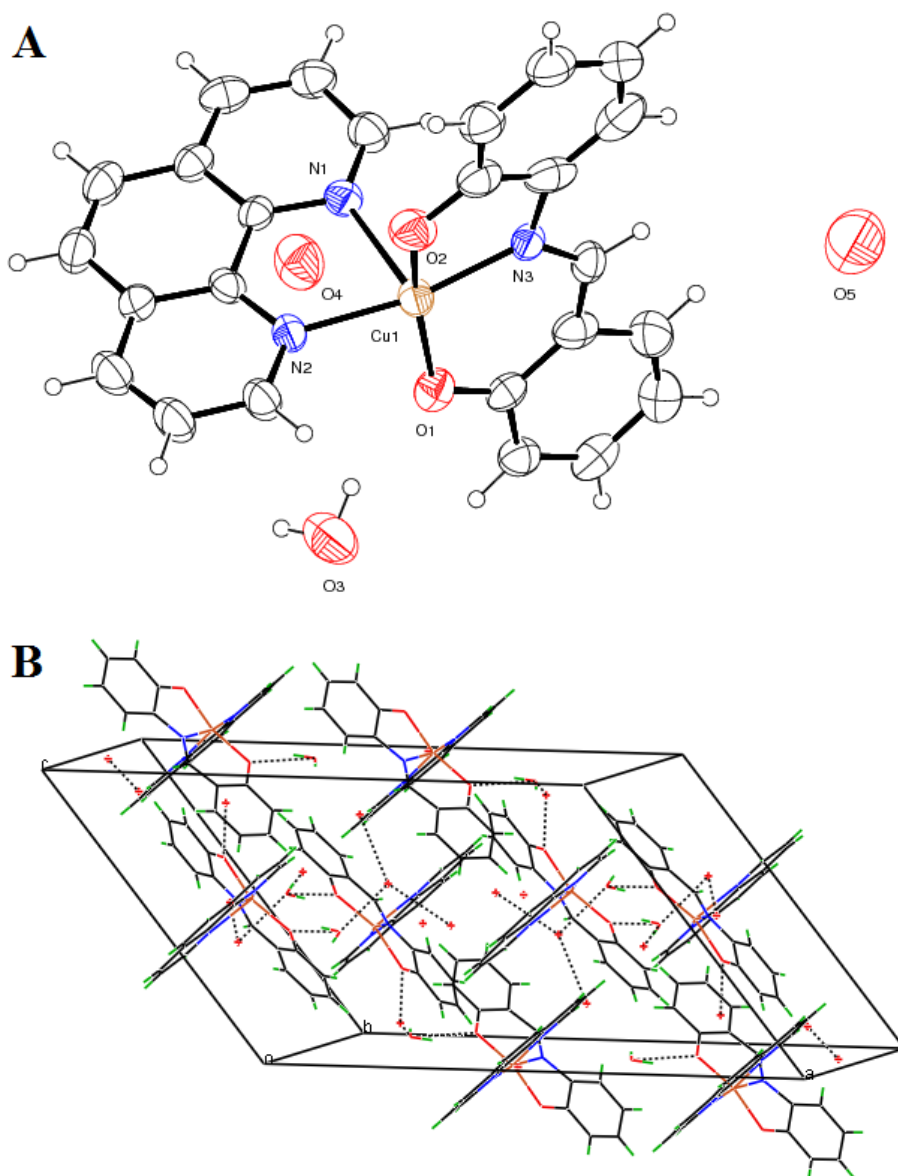


**Fig. 1.** (A) ORTEP diagram of the compound **1** and (B) packing of the molecules in the unit cell. Bond lengths [ $\text{\AA}$ ] and angles [ $^\circ$ ] for **1**: N(1)-Cu(1) = 2.287(5); N(2)-Cu(1) = 2.016(5); N(3)-Cu(1) = 1.904(12); N(3')-Cu(1) = 1.981(17); O(1)-Cu(1) = 1.915(4); O(2)-Cu(1) = 1.933(4); N(3)-Cu(1)-O(1) = 100.8(5); N(3)-Cu(1)-O(2) = 78.2(5); O(1)-Cu(1)-O(2) = 162.51(18); O(1)-Cu(1)-N(3') = 76.5(6); O(2)-Cu(1)-N(3')

= 101.9(6); N(3)-Cu(1)-N(2) = 167.6(4); O(1)-Cu(1)-N(2) = 91.41(17); O(2)-Cu(1)-N(2) = 90.85(19); N(3')-Cu(1)-N(2) = 167.2(6); N(3)-Cu(1)-N(1) = 97.7(3); O(1)-Cu(1)-N(1) = 100.14(16); O(2)-Cu(1)-N(1) = 97.29(17); N(3')-Cu(1)-N(1) = 100.0(4); N(2)-Cu(1)-N(1) = 77.79(18).

The Cu atom is five-coordinated. The geometry of coordination is approximately square pyramidal with O1N3O2N2 atoms forming the basal plane for Cu1. The apical N(1)-Cu(1) bond length is found to be much longer (2.287(5) Å) than the other two Cu-N distances (N(2)-Cu(1) = 2.016(5) and N(3)-Cu(1) = 1.904(12)). All the hydrogens could be located in the difference Fourier map. However, it was decided to fix the hydrogens at geometrically meaningful positions. These atoms were refined by riding model. The packing of molecules in the unit cell shows water molecules mediated H-bonding interactions stabilizing the lattice. Compound **2**, on the other hand, crystallizes in orthorhombic system with space group  $Pca2_1$  and lattice parameters  $a = 9.3659(6)$  Å,  $b = 17.4585(11)$  Å,  $c = 18.1049(13)$  Å,  $\alpha = 90^\circ$ ,  $\beta = 90^\circ$ ,  $\gamma = 90^\circ$ . The bond length and bond angles are given in Table S2 of the Supplementary material.

Fig. 2 shows the ORTEP representation of the molecule with 40% probability ellipsoids [18] and the packing of the molecules. There are two molecules in the asymmetric unit. Cu atoms of both molecules (Cu1 and Cu2) have near square-planar coordination with two nitrogen atoms *trans*- to each other, one imine N of the Schiff base ligand and the tertiary N of the imidazole, and two phenolate O of the Schiff base ligand. The Cu(1)-N(2) bond length is slightly longer than that with imine N(1). As

expected, Cu(1)-O(1) is found to be longer than Cu(1)-O(2) bond length showing the difference in formation of five-membered ring for the former versus six-membered ring in the latter case. The bond angles clearly show the molecule is not completely planar. The mean plane calculation of the basal square plane coordination shows the coordinating N and O atoms to have small tetrahedral distortion (from the ideal square plane). The packing of molecules in the unit cell shows imidazole mediated H-bonding interactions as well as the intermolecular  $\pi$ -stacking interactions of aromatic rings of the Schiff base are operating in stabilizing the lattice.

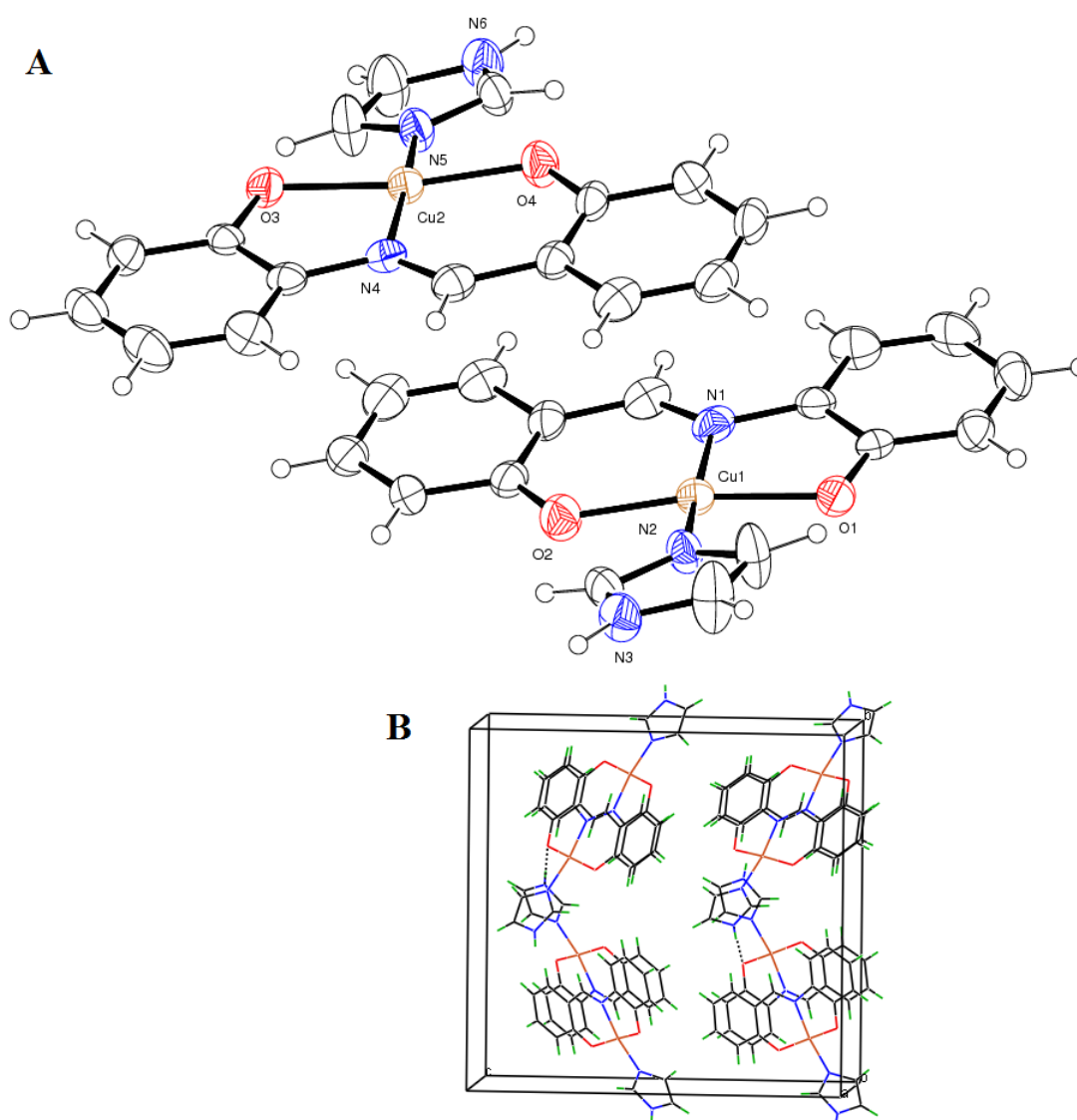


**Fig. 2.** (A) ORTEP diagram of the compound **2** and (B) packing of the molecules in the unit cell. Bond lengths [ $\text{\AA}$ ] and angles [ $^\circ$ ] for **2**: N(1)-Cu(1) = 1.943(11); N(2)-Cu(1) = 1.953(7); O(1)-Cu(1) = 1.927(6); O(2)-Cu(1) = 1.890(7); N(4)-Cu(2) = 1.926(9); N(5)-Cu(2) = 1.965(7), O(3)-Cu(2) = 1.932(6); O(4)-Cu(2) = 1.888(6); O(2)-Cu(1)-O(1) = 169.6(3); O(2)-Cu(1)-N(1) = 94.7(4); O(1)-Cu(1)-N(1) = 84.4(3); O(2)-Cu(1)-N(2) = 89.9(3); O(1)-Cu(1)-N(2) = 92.3(3); N(1)-Cu(1)-N(2) = 171.3(4).

## 2.2. EPR results

The EPR spectra at X-band frequency for the compounds **1** and **2** in powder state as well as in DMF solution were recorded at room temperature (RT), and the DMF frozen glass spectra were recorded at liquid nitrogen temperature (LNT) and are shown in Fig. 3. In general, both the compounds containing Cu(II) as the central metal ion display strong spectra since they are EPR sensitive with its characteristic g-values and hyperfine splitting in the frozen state and at RT when the solid compounds are dissolved in DMF medium. It is noteworthy that RT spectra of both solids (Figs. 3a and b) exhibit excessively broad lines for reasons of strong dipolar interactions between the adjacent Cu(II) centres as indicated by the nature of packing in Figs. 1 and 2 above. The EPR of their DMF solutions as shown in Figs. 3c and d are nothing but a simple 4-line spectra due to  $I=3/2$  from  $^{63,65}\text{Cu}$  nuclei with no exhibition of resolution from the two different isotopes but with a strong  $m_I$  dependent line width. The isotropic g-value for compounds **1** and **2** are 2.1 and 2.085 with the respective isotropic hyperfine splitting 7.3 and 8.5 mT as shown in Table 1. These values are characteristic of approximately planar or tetragonal crystal field environment.

The most notable results, however, come from their frozen solution spectra indicating their differences in structure where the compound **1** is axial in character and **2** has a rhombic symmetry. The axial character of compound **1** is confirmed by the observation of only two anisotropic  $g$ -values viz.  $g_{\parallel} = 2.21$  and  $g_{\perp} = 2.09$  (Fig. 3e) along with the resolved hyperfine parallel component ( $A_{\parallel}$ ) due to  $^{63,65}\text{Cu}$  and with no resolution of the same in the perpendicular section due to  $A_{\perp}$  being less than its line width. This justifies the crystallographic prediction of its axial character with the planar unit of  $\text{Cu}(\text{O1N3O2N2})$  along with the long apical bond of  $\text{N}(1)\text{-Cu}(1)$ . On the other hand, the EPR of compound **2** ( Fig.3f) is clearly rhombic in nature with  $g_{11} = 2.21$ ,  $g_{22} = 2.09$ , and  $g_{33} = 1.97$  with  $g_{\text{av}}$  working out to 2.09, very close to that of  $g_{\text{iso}}$  being 2.085 which again justifies the rhombic character of the molecule as recognized by crystallography. Similar anisotropy is noted in the corresponding hyperfine values,  $A_{11} = 19.9$  mT,  $A_{22} \approx 7.0$  mT, and  $A_{33} <$  line width, an average of which makes  $A_{\text{av}} \approx 9.62$  mT with the assumption of  $A_{33} \approx 2.0$  mT (less than the line width) which is fairly close to the observed  $A_{\text{iso}}$  of 8.5 mT. The  $g_{\text{av}}$  values calculated from the corresponding polycrystalline values at RT slightly differ from those of  $g_{\text{av}}$  observed for the DMF frozen solution suggesting that DMF may have played a minor role in disturbing the ligand environment of the molecule when brought into solution. However, it is gratifying to see that EPR conforms to the crystallographic structures of both compounds, one being axial and the other being rhombic in their character. All observed EPR parameters are presented in Table 1.

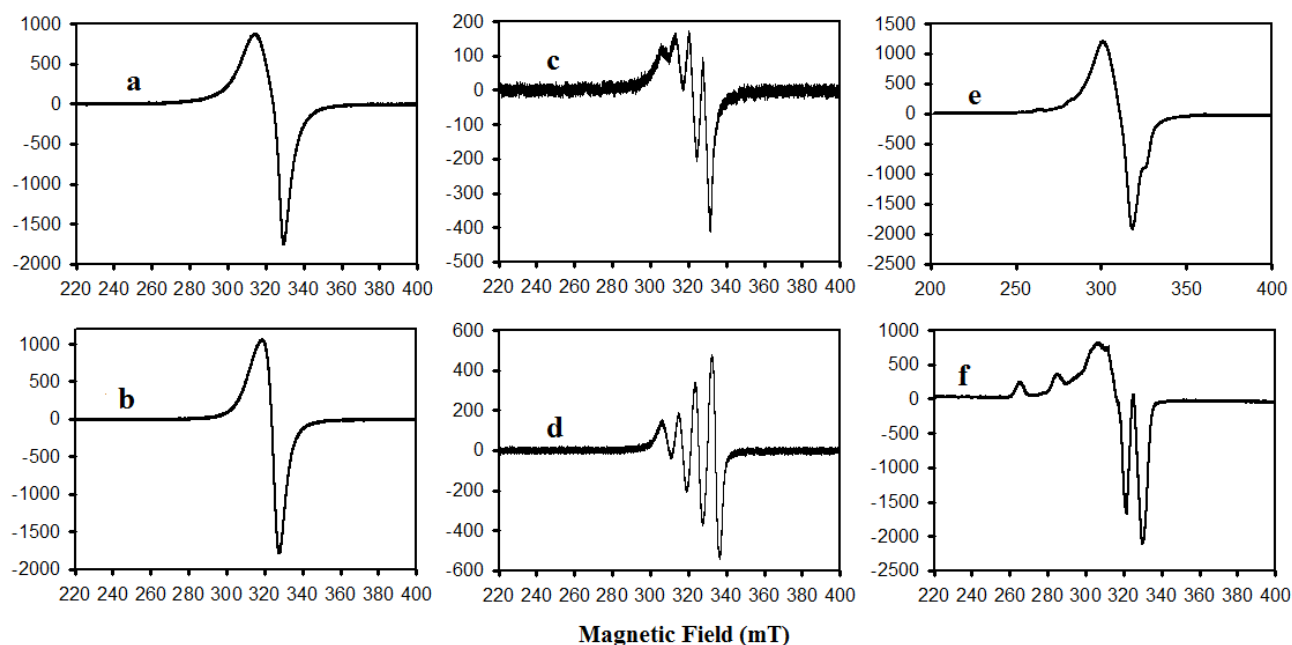


**Fig. 3.** X-band EPR spectra of the compounds. (a)-(b) are RT spectra for **1-2** powder samples, (c)-(d) are RT solution spectra for **1-2** in DMF, and (e)-(f) are LNT frozen glass spectra for **1-2** in DMF, respectively.

**Table 1.** EPR parameters for compounds **1** and **2** derived from the spectra at RT and LNT.

Compound/state/temp.	$\nu$ (GHz)	g value	HFS values (mT)
<b>1</b> - DMF frozen glass at LNT	9.138	$g_{\parallel} = 2.21$ $g_{\perp} = 2.09$	$A_{\parallel} = 20.67$ $A_{\perp} < \text{linewidth}$
<b>1</b> - DMF solution at RT	9.434	$g = 2.11$ $\Delta_{pp} \approx 4.4$ to 3.9mT	$A_{\text{iso}} = 7.30$
<b>1</b> - Powder at RT	9.447	$g_{\parallel} = 2.14$	Not resolved

		$g_{\perp} = 2.06$	
<b>2-</b> DMF frozen glass at LNT	9.137	$g_{zz} = 2.21$ $g_{yy} \approx 2.09$ $g_{xx} = 1.97$	$A_{zz} = 19.99$ $A_{yy} \approx 7.0$ $A_{xx} < \text{linewidth}$
<b>2-</b> DMF solution at RT	9.433	$g = 2.085$ $\Delta_{pp} \approx 4.6$ to 4.13 mT	$A_{iso} = 8.50$
<b>2-</b> Powder at RT	9.448	$g_{11} = 2.11$ $g_{22} = 2.07$ $g_{33} = 2.05$	Not resolved

### 2.3. DNA binding studies

DNA binding studies were performed using UV-Vis spectroscopy. Electronic absorption titration experiments were performed with incremental amounts of calf thymus DNA (CT-DNA) in 10 mM Tris-HCl buffer (pH 7.54) by keeping the individual complex concentration constant at  $2.5 \times 10^{-4}$  M. Absorption spectrum of the complex **1** and **2** in the absence and presence of CT-DNA has been shown in Fig. 4. On addition of CT-DNA both the complexes show a decrease in molar absorptivity (hypochromism of 47.5% for **1** and 82.5 % for **2**) of the  $\pi \rightarrow \pi^*$  absorption band indicating strong binding of the complexes to DNA. These changes are typical of complexes that bind to DNA by intercalation mode, which involves strong stacking

interaction between aromatic chromophore and the DNA base pairs [19]. To determine the quantitative comparison of the DNA binding ability, we determined the intrinsic binding constant,  $K_b$ , of the complexes for binding with calf thymus (CT-DNA) by using the following Eq. (1).

$$\frac{[DNA]}{(\varepsilon_a - \varepsilon_f)} = \frac{[DNA]}{(\varepsilon_b - \varepsilon_f)} + \frac{1}{K_b(\varepsilon_b - \varepsilon_f)} \quad (1)$$

where, [DNA] is the concentration of CT-DNA used, and  $\varepsilon_a$ ,  $\varepsilon_f$  and  $\varepsilon_b$  correspond to apparent extinction coefficients for the complex i.e., Abs/[complex] in the presence of DNA, in the

absence of DNA and to fully bound DNA, respectively. A plot of [DNA]/( $\varepsilon_a - \varepsilon_f$ ) versus

[DNA] yields a slope =  $1/(\varepsilon_b - \varepsilon_f)$ , and the intercept =  $1/K_b(\varepsilon_b - \varepsilon_f)$ , respectively. The binding constant  $K_b$  is calculated from the ratio of the slope to the intercept. The  $K_b$  values are  $1.53 \times 10^5 \text{ M}^{-1}$  for **1** ( $R^2 = 0.99770$  for 12 points) and  $3.13 \times 10^5 \text{ M}^{-1}$  for **2** ( $R^2 = 0.99867$  for 9 points), respectively. These values are comparable to that reported for a classical intercalator such as ethidium bromide ( $K_b = 1.40 \times 10^5 \text{ M}^{-1}$ ) in 25 mM Tris-HCl buffer (pH 7.33) [20]. The high percentage (82.5 %) of hypochromism and the higher  $K_b$  value for **2** compared to **1** indicates its higher binding propensity which arises due to the four coordinate square planar structure of **2**, which allows the intercalating ligand to insert into the DNA base pair effectively [21-22], and this enhanced stacking interaction results in increased binding ability. It is to be noted that

$K_b$  of this neutral complex **2** is higher than that for the reported four coordinate cationic compound  $[\text{Cu}(\text{pabt})(\text{Imz})]\text{ClO}_4$  containing imidazole along with the chelating NNS donor ligand [16]. Table S3 (Supplementary material) shows a comparison of  $K_b$  values with some more analogous compounds reported in literature.

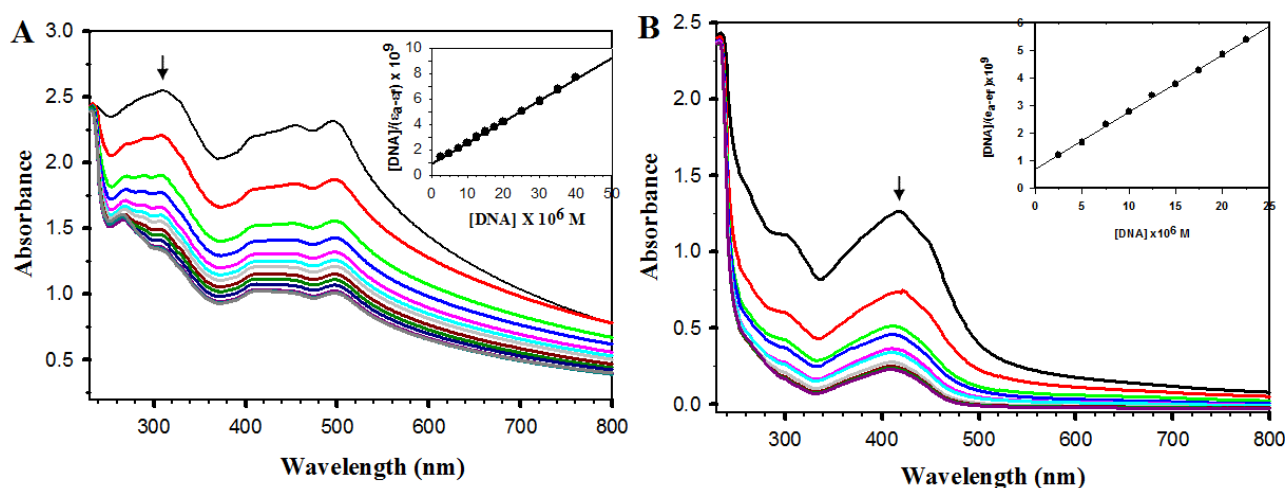


**Fig. 4.** (A) Change in electronic absorption spectra of **1** [ $2.5 \times 10^{-4}$  M] upon titration with CT-DNA (0–40  $\mu\text{M}$ ) dissolved in 10 mM Tris–HCl buffer (pH 7.54). (B) Change in electronic absorption spectra of **2** [ $2.5 \times 10^{-4}$  M] upon titration with CT-DNA (0–25  $\mu\text{M}$ ) dissolved in 10 mM Tris–HCl buffer (pH 7.54). Arrow shows the decrease in absorbance with respect to an increase in the concentration of CT-DNA. The figure in inset shows the linear fit of  $[\text{DNA}]/(\epsilon_a - \epsilon_f)$  versus  $[\text{DNA}]$ . The binding constant ( $K_b$ ) was calculated using the Eq. (1).

#### 2.4. Viscosity measurements

As supporting evidence to the spectroscopic analyses of DNA intercalation exhibited by both the compounds, viscosity measurements on CT-DNA by varying the concentration of added complex were also conducted. Normally it is observed that the relative viscosity of CT-DNA solution increases on interaction with substrates that

bind by intercalative mode. This is because insertion of metal complex between the DNA base pairs causes the base pairs to separate which increases the overall length of DNA, thus resulting in an increase in viscosity of DNA. The effect of addition of increasing amount of complex **1** and **2** on the relative viscosity depicted in Fig. 5 shows steady increase in the viscosity of the DNA which clearly suggests intercalative mode of binding of the complexes to DNA. It is also to be noted that the increase in viscosity is more pronounced in case of **2**. The results support the spectral studies which suggest that complex **2** binds more strongly to CT-DNA.

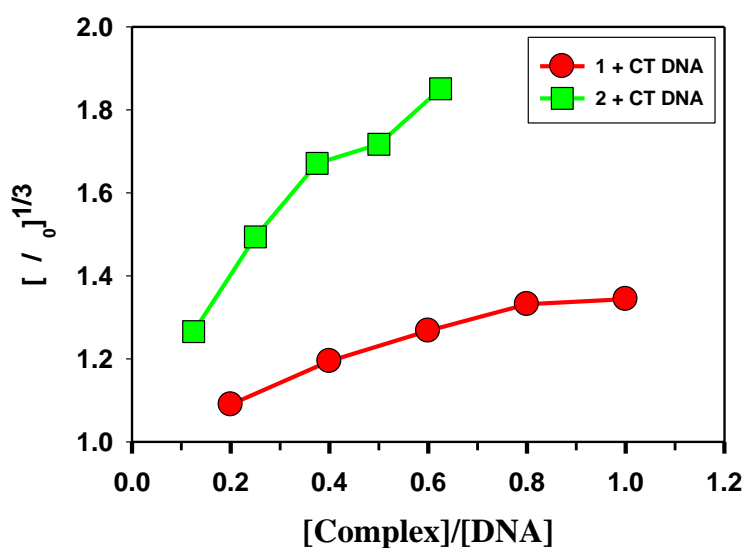


**Fig. 5.** Effect of increasing amount of complex **1** (red circles) and **2** (green squares) on the relative viscosity of CT-DNA (100  $\mu$ M) at room temperature in 10 mM Tris.HCl buffer (pH7.46).

## 2.5. Results on biological activity

### 2.5.1. Cytotoxicity

The cytotoxicity profiling of the compounds **1** and **2** were evaluated by MTT assay using A549 lung cancer cell line, MCF7 breast cancer cell line, L132 human lung

embryonic normal cell line and human keratinocyte HaCaT normal cell line. The cell viability was determined by the reduction of yellow MTT into purple formazan product by the enzymatic activity of mitochondrial dehydrogenase in the live cells. A concentration dependent effect on the cell viability was observed (Fig. 6) for both cancerous cell lines (MCF7 and A549) as well as normal cell lines (HaCaT, L132). Results indicate that even at as low concentration as 0.25  $\mu\text{M}$ , both the compounds **1** and **2** are found to be toxic to A549 cells as indicated from their respective cell viability of 88% and 67%, while toxicity is comparatively much less in normal cells HaCaT at the same dose (cell viability is 97% for **1** and 91% for **2**), and almost no toxicity was observed for L132 lung normal cells that were treated with 0.25  $\mu\text{M}$  of **1** and **2** (Fig. 6). The viability of A549 cells treated with 0.5  $\mu\text{M}$  of **1** and **2** falls to 69.5% and 54%, respectively, as compared to cell viability of 93% in case of L132 cells treated with same dose of **1** or **2**. Also **1** shows similar results in normal cell HaCaT as indicated by 91% cell viability at 0.5  $\mu\text{M}$  dose. Similar observation were found when A549 cells were treated with 1  $\mu\text{M}$  dose of **1** and **2**, cell viability was reduced to 38% for both compounds, whereas the compounds appear to be much less toxic to L132 normal cells showing cell viability of 78% and 86%, respectively, on treatment with 1  $\mu\text{M}$  dose of **1** and **2**. Though cell viability seems fairly moderate (50%) when normal HaCaT cells are treated with 1  $\mu\text{M}$  dose of **1**, compound **2** proved to be highly toxic to HaCaT cells at the same 1  $\mu\text{M}$  dose. Again remarkable difference in cell viability is observed when compared the effect of the 2.5, 5 and 10  $\mu\text{M}$  dose of compounds **1** and **2** on lung cancer A549 cell lines versus L132 lung normal cells (Fig. 6). In MCF7 cell line, compound **1** is found to be more toxic than **2** for the entire concentration range

tested, but found to be much less toxic as compared to that for A549 cells. However, both **1** and **2** are found to be very toxic toward HaCaT cells for their concentrations of 2.5  $\mu\text{M}$  and higher, but at 1.0  $\mu\text{M}$  concentration, **1** is found to be remarkably less toxic than **2** as revealed from their cell viabilities of 49.5% and 14.1% for **1** and **2**, respectively (Fig. 6).

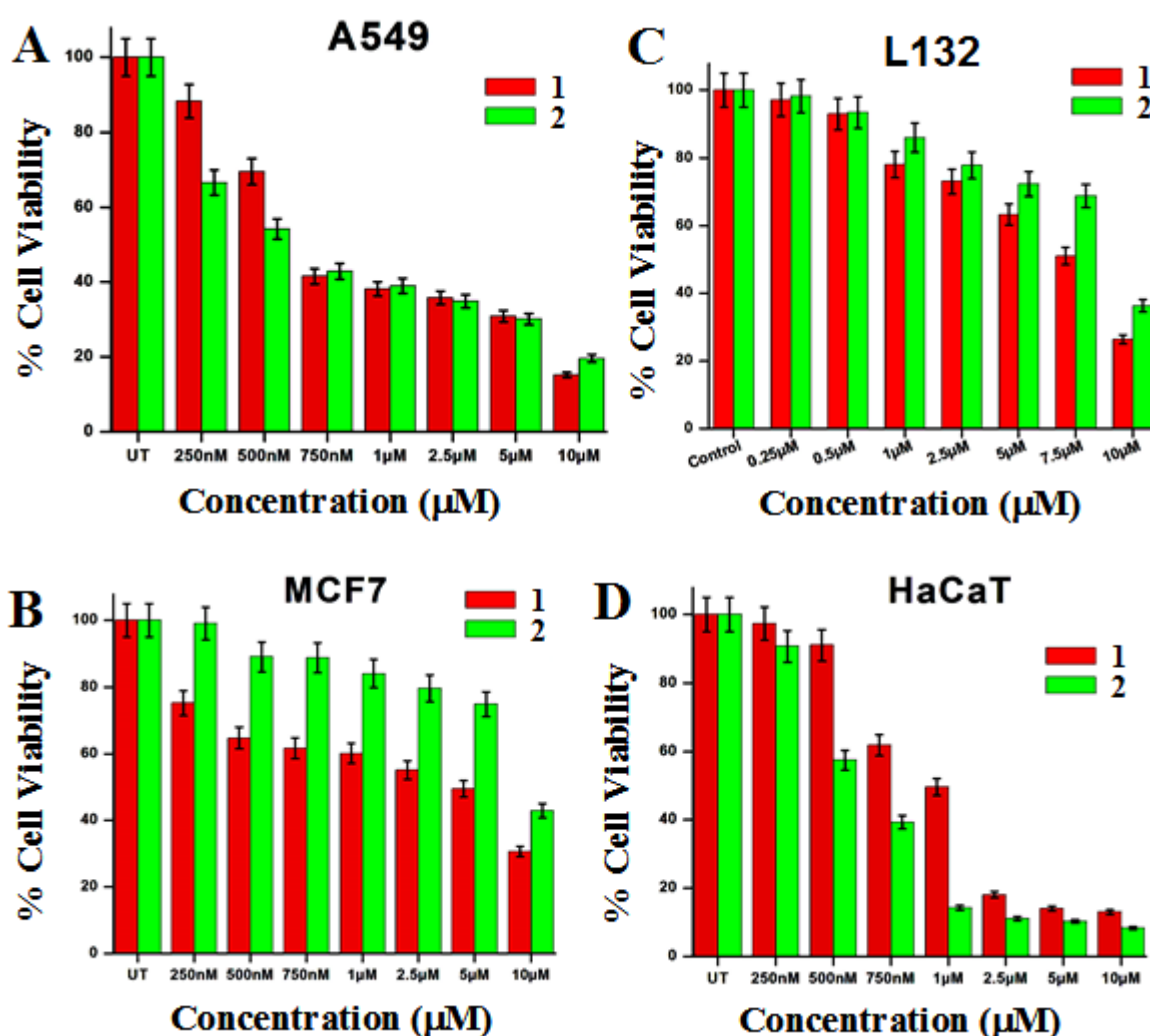


**Fig. 6.** MTT assay for the compounds **1** and **2**. Panel A. A549 cell line, panel B. MCF7 cell line, panel C. L132 cell line, and panel D. HaCaT cell line.

The plot of cell viability versus concentrations of the compounds **1** and **2** for all these cell lines is shown in Fig. S5 (Supplementary material). The  $\text{IC}_{50}$  values for **1** and **2**

calculated from this plot for both the cancer cell lines A549 and MCF7 and for the two normal cell lines are presented in Table 2.

**Table 2.** IC<sub>50</sub> values for the compounds **1** and **2** calculated from the plot of cell viability versus concentration in the MTT assay.

Cell line	IC <sub>50</sub> (μM) for	
	Compd. <b>1</b>	Compd. <b>2</b>
A549	0.67	0.59
MCF 7	6.30	8.88
L132	7.60	8.95
HaCaT	0.99	0.60

It is to be noted here that the IC<sub>50</sub> values for A549 cells are better than the IC<sub>50</sub> value reported for cisplatin (4.13 μM for A549). On the other hand, the IC<sub>50</sub> values for **1** and **2** for MCF7 cell line are found to be slightly higher than that reported for cisplatin (3.92 μM for MCF7) and much lower than that reported for carboplatin (36.65 μM for MCF7) [3c]. It is to be noted here that recently we have reported [15] a few Cu(II)/Zn(II) complexes with a carbohydrazone ligand along with 1,10-phenanthroline as a coligand which were found to be very promising anticancer agents tested for the human lung cancer A549 cell line and for the breast cancer MCF7 cell line as revealed from their IC<sub>50</sub> values. However, those Cu(II) compounds were found to be very toxic for the normal L132 and HaCaT cell lines also [15]. In contrast, the two compounds under present study are found to be much less toxic toward normal L132 cell lines,

suggesting their suitability as anticancer agents specifically for human lung cancer A549 cell line.

In order to assess the significance of our results, the  $IC_{50}$  values and  $K_b$  values of both **1** and **2** have been compared with those of some recently reported copper (II) complexes for A549 and MCF7 cell lines and presented in Table S4 of the Supplementary material. The comparison reveals that **1** and **2** exhibit higher value of intrinsic binding constant  $K_b$  as well as exhibits better cytotoxic response in A549 cell line (as indicated by their lower  $IC_{50}$  values) than most of the reported copper complexes. Two of the Cu complexes reported by Nagababu and coworkers [1a] show similar low  $IC_{50}$  values in A549 cell line, however, these complexes are reported to be cytotoxic toward both cancerous and normal cell lines. Cu(II) complexes reported by Lu et. al [3c] do exhibit lower  $IC_{50}$  values in A549 as well as MCF7 cell lines, however, they have not reported cytotoxic effect on any normal cell line. The complexes **1** and **2** in this study have been tested in both cancerous and noncancerous cell lines and showed remarkable difference in cytotoxicity in lung cancer A549 cell line as compared to human lung normal cell line L132, suggesting their potential to serve as anticancer therapeutic agents. To compare the relative antiproliferative effect of **1** and **2** on cancerous versus normal cells, their therapeutic index (TI) has been calculated from the ratio of the  $IC_{50}$  values of the complexes in normal cells to that in cancer cells and has been presented in supporting information Table S5.

### 2.5.2. Dual-Fluorescence Viability: AO/PI Dual Staining assay for A549 and L132 cells

This dual staining assay using the fluorescence microscopy is used to analyze the induction of cell apoptosis in presence of the compounds **1** and **2**, with the help of acridine orange (AO) and propidium iodide (PI) nucleic acid binding dyes. AO is permeable to both live and dead cells, staining all nucleated cells to generate green fluorescence. On the other hand, PI enters only in dead, dying, and necrotic nucleated cells with compromised membranes and stains them all generating red fluorescence. But when cells are stained with both AO and PI together, all dead nucleated cells fluoresce red and all live nucleated cells fluoresce green due to Förster resonance energy transfer (FRET). The following morphological changes were observed (Figs. 7 and 8) in the treated cells using this staining method: (a) the viable cells with highly organized nuclei fluoresce green as seen from all the control in Figs. 7 and 8; (b) early apoptotic cells with nuclear condensation, that emit orange-green fluorescence, observed in the treatment with 2.5 and 5  $\mu$ M concentrations of the respective compounds; (c) late apoptotic cells with highly condensed or fragmented chromatin and fluoresce orange to red, observed in the treatment with 2.5 and 5  $\mu$ M concentrations of the respective compounds; and (d) necrotic cells fluoresce red with no indication of chromatin fragmentation as clearly evident (Figs. 7 and 8) in the cases of A549 cells treated with 5  $\mu$ M of each of **1** and **2**, while such red fluorescence is not observed for L132 (Figs. 7 and 8) cells with 1-5  $\mu$ M concentrations for **1** and **2** suggesting no or very little DNA damage at these concentrations. These results are

consistent with the cell viability observed from their MTT assay (Fig. 6), confirming the marked differences in the cell death in A549 and L132 cells treated with both **1** and **2**, and these morphological changes indicate that both the complexes might have induced cell death via both apoptosis and necrosis [3e, 23].

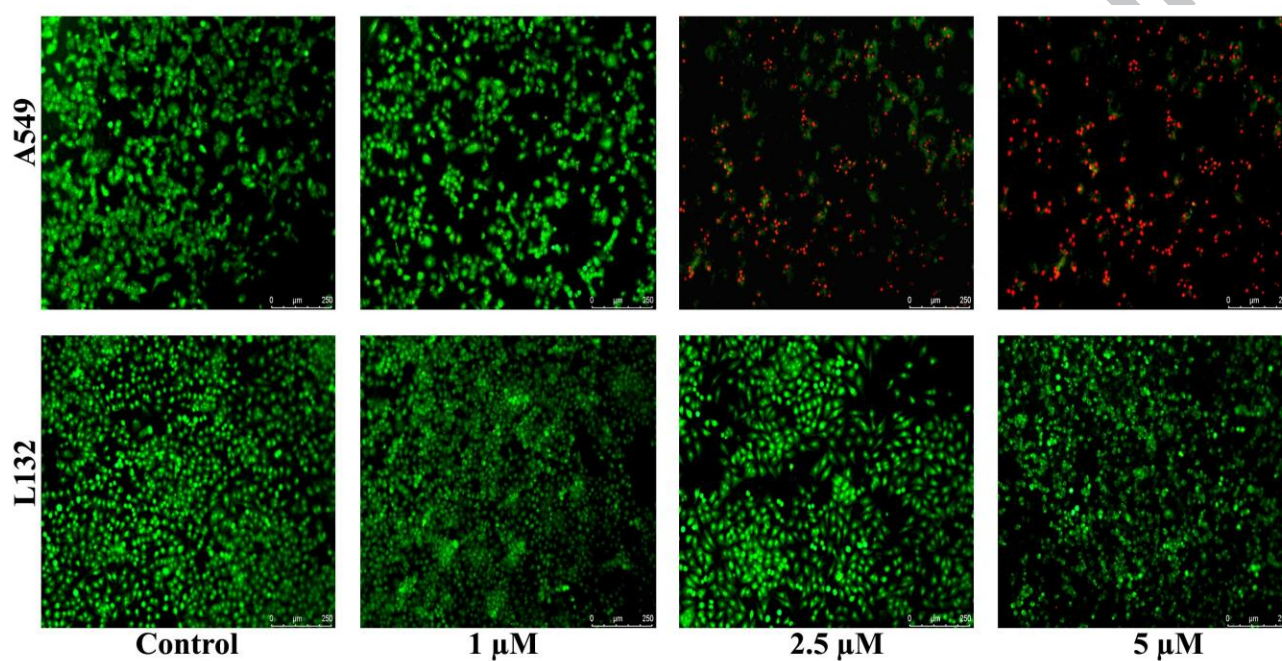


**Fig. 7.** AO/PI staining results for compound **1** with A549 and L132 cell lines. Scale bar: 250  $\mu\text{m}$ .

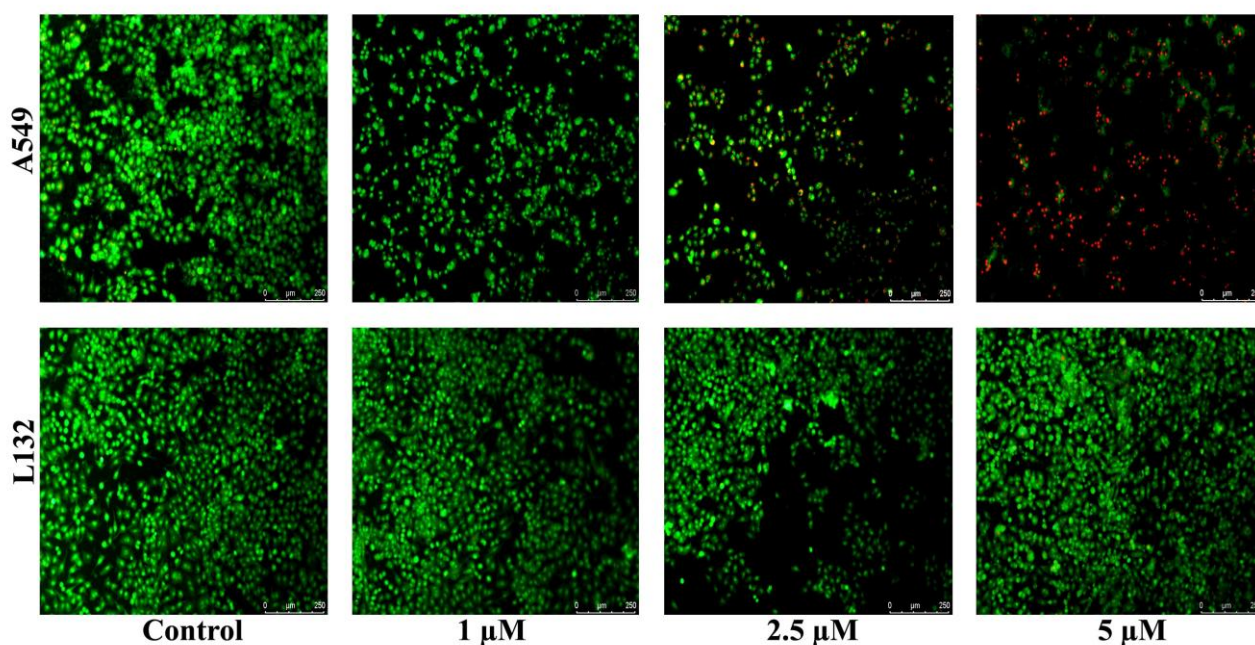


**Fig. 8.** AO/PI staining results for compound **2** with A549 and L132 cell lines. Scale bar: 250  $\mu$ m.

It is to be pointed out here that though the DNA binding experiments carried out *in vitro* showed that the two compounds under study are capable of DNA intercalation, it does not imply that the cell apoptosis observed are originating from this intercalation, because it will largely depend on the structural integrity of these complexes after entering the cell membrane. Though this possibility cannot be completely ruled out at this stage, there could be other possibilities that they may undergo reduction to Cu(I) in the reducing environment after entering the cell membrane [23e-h] followed by ligand dissociation (as reflected from their electrochemical behavior) and may, in turn, either interact with proteasome [2d] causing apoptosis or may combine with dioxygen generating reactive oxygen species (ROS) which may cause oxidative cleavage of DNA polynucleotide chains leading to apoptosis [1b]. This could be the reason for these two compounds behave differently from other reported compounds [1b, c]. It should be mentioned here in this context that cancer cells are more sensitive to proteasome inhibition than normal cells [1b], at the same time it is also true that cancer cells in general have increased levels of reactive oxygen species (ROS) compared to normal cells. Thus, it is equally probable that the generated Cu(I) species with a changed ligand environment may either cause proteasome inhibition leading to cell death or escalate the level of ROS to a toxic level that results in oxidative stress-induced cell death. This is the most plausible explanation we can give with the currently available experimental evidences.

It is to be noted here that the cytotoxicity study of the free Schiff base ligand N-salicylidene-*o*-aminophenol was also carried out using the human lung cancer A549 cell line with different concentrations (2.5  $\mu\text{M}$ , 5  $\mu\text{M}$ , 7.5  $\mu\text{M}$  and 10  $\mu\text{M}$ ) of the free ligand for 24 hours. No cell death was observed with 2.5  $\mu\text{M}$  concentration of the free ligand. The cell viabilities were found to be nearly 96.5 % with 5  $\mu\text{M}$ , 95.5 % with 7.5  $\mu\text{M}$  and about 91 % with 10  $\mu\text{M}$  of the free ligand, respectively (Fig. S6, Supplementary material), suggesting that the free ligand is capable of causing about 9-10% cell death in the presence of 10  $\mu\text{M}$  concentration of the free ligand. Thus, the toxicity observed for the compounds **1** and **2** (e.g., with the concentrations 5  $\mu\text{M}$  and 10  $\mu\text{M}$ , respectively) may have some small contribution from the free Schiff base ligand, provided the compounds undergo ligand dissociation after entering the cell membrane, otherwise the observed toxicity should be accounted for the complex as a whole.

### 2.6. Electrochemical results

The electrochemical behaviour of compounds **1** and **2** have been studied in DMF containing 0.1 M  $[\text{N}(n\text{-Bu})_4]\text{ClO}_4$  at a platinum working electrode using cyclic voltammetry (CV) in dinitrogen atmosphere. The cyclic voltammetric behaviour of both the compounds are found to be independent of scan directions, and yield oxidation and reduction peaks almost in similar positions irrespective of the scan direction (Fig. 9, panels A and B for **1**, and panels C and D for **2**, respectively). For an initial negative scan compound **1** shows (Fig. 9) a broad reduction wave near 1.25 V, reversal of this scan yields three successive oxidations waves at 0.78, +0.839 and

+1.17 V, respectively, further reversal of the scan yields reduction waves at +0.73 and +0.08 V, when scanned within -1.5 to +1.5 V. Compound **2** shows a broad reduction wave near -1.53 V (versus Ag/AgCl), a weak oxidation peak at -1.20 V followed by another oxidation peak near -0.0832 V is observed on scan reversal. Further positive scan shows oxidation wave near +0.88 V, reversal of this scan yielded three successive reduction waves at +1.26, +0.778 and +0.3168 V, respectively. The reduction peak at -0.0832 V is coupled to the oxidation wave at +0.3168 V indicating a quasi-reversible redox process. Thus the absence of any reversible or nearly reversible Cu(II)/Cu(I) redox couple in the cyclic voltammograms of these complexes suggests that they undergo irreversible oxidation and reduction involving both metal center and ligand center, and any of them does not retain the same geometry in both these oxidation states as it is known that only a reversible or nearly reversible Cu(II)/Cu(I) redox couple retain almost same geometry in both these oxidation states because the redox potentials of Cu(II)/Cu(I) systems depend on the relative thermodynamic stabilities of the two oxidation states in a given ligand environment [16, 17].

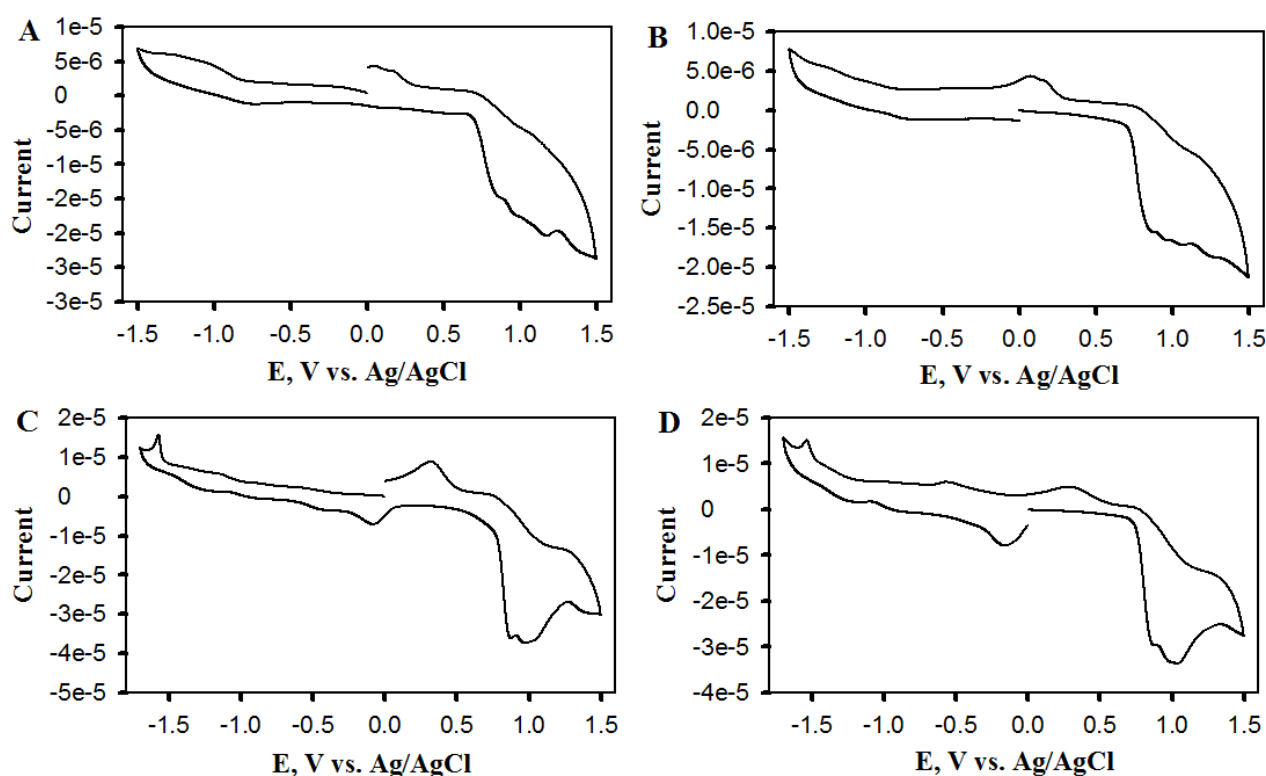


**Fig. 9.** Cyclic voltammogram of the compounds ( $1.25 \times 10^{-3} \text{ mol L}^{-1}$ ) in DMF containing 0.1 M  $[\text{N}(\text{n-Bu})_4]\text{ClO}_4$  at a scan rate of  $100 \text{ mV s}^{-1}$ . Panels A and B for **1**, panels C and D for **2**, for initial negative and positive scans, respectively.

### 3. Conclusions

Both the compounds efficiently bind to DNA by intercalation mode with binding constants  $1.53 \times 10^5 \text{ M}^{-1}$  and  $3.13 \times 10^5 \text{ M}^{-1}$ , respectively, as revealed from their DNA binding study with calf thymus DNA. The compounds **1** and **2** exhibit in vitro cytotoxicity against human breast cancer MCF7 cell line and human lung cancer A549 cell line and they are found to be highly potent for A549 cell line in particular as revealed from their  $\text{IC}_{50}$  values. At the same time they are found to be much less toxic for the L132 human lung embryonic normal cell line. AO/PI dual staining results

strongly suggest the induction of both apoptotic and necrotic cell death pathways for the anticancer activity of these complexes.

## 4. Experimental

### 4.1. Chemicals

*o*-Aminophenol, imidazole and salicylaldehyde were obtained from Aldrich. Calf thymus DNA was obtained from Sigma-Aldrich (USA), *N,N*-dimethylformamide (DMF, GR), absolute ethanol, methanol (GR), DMSO, 1,10-phenanthroline monohydrate and  $\text{Cu}(\text{OAc})_2 \cdot \text{H}_2\text{O}$  (GR) were obtained from Merck.

4.2. Preparation of *N*-salicylidene-*o*-aminophenol ( $H_2L$ ). This Schiff base of *o*-aminophenol and salicylaldehyde was prepared following the reported method [16b]. Yield 75%. Anal. Calc. for  $\text{C}_{13}\text{H}_{11}\text{NO}_2$ : C, 73.22; H, 5.20; N, 6.56. Found: C, 73.12; H, 5.21; N, 6.54%.

### 4.3. Preparation of the complexes

4.3.1.  $[\text{CuL}(\textit{o}\text{-phen})]$  (**I**). 1,10-phenanthroline (*o*-phen) monohydrate (0.398 g, 0.002 mol) in methanol (10 mL) was slowly added to a solution of  $\text{Cu}(\text{OAc})_2 \cdot \text{H}_2\text{O}$  (0.399 g, 0.002 mol) in methanol (20 mL, 23 °C) during 30 min with stirring at room temperature. Then this reaction mixture was slowly added to a solution of *N*-(salicylidene)-*o*-aminophenol (0.426 g, 0.002 mol) in methanol (30 mL, ~ 25 °C) during 30 min with stirring at RT. A dark blue compound separated from the solution. The solid was filtered, washed well with methanol, then with water and finally again with methanol and dried in vacuo. This compound was recrystallized from  $\text{CH}_3\text{OH}:\text{CH}_3\text{CN}$  (1:1) at RT while suitable single crystals were obtained. This compound has been characterized by X-ray crystallography. This is to be noted here

that on long standing (or in vacuum) these crystals lose their water of crystallization and become amorphous. *Anal. Calc.* for  $C_{25}H_{17}N_3O_2Cu$ : C, 65.99; H, 3.77; N, 9.24.

Found: C, 66.01; H, 3.80; N, 9.23%. ESI-MS in  $CH_3CN$ :  $m/z$  454.30  $[M]^+$ ,  $m/z$  491.30  $[(M+K)-2H]^+$ .

4.3.2.  $[CuL(Imz)]$  (2). Imidazole (0.136 g, 0.002 mol) in methanol (10 mL) was slowly added to a solution of  $Cu(OAc)_2 \cdot H_2O$  (0.398 g, 0.002 mol) in methanol (20 mL,  $\sim 5$  °C) during 20 min with stirring at room temperature ( $\sim 23$  °C) while a dark blue solution was obtained. Then this solution was slowly added to a solution of N-(salicyldene)-*o*-aminophenol (0.426 g, 0.002 mol) in methanol (30 mL,  $\sim 25$  °C) during 30 min with stirring at RT. A green compound separated from the solution. The solid was filtered, washed well with methanol and dried in vacuo. This compound was recrystallized from  $CH_3CN:CH_3OH$  (1 : 1) at RT while suitable single crystals were obtained. This compound has also been characterized by X-ray crystallography.

*Anal. Calc.* for  $C_{16}H_{13}N_3O_2Cu$ : C, 56.05; H, 3.82; N, 12.26. Found: C, 56.01; H, 3.87; N, 12.31%. ESI-MS in  $CH_3CN$ :  $m/z$  343.01  $[M]^+$ ,  $m/z$  344.81  $[M+2H]^+$ .

#### 4.4. Physical measurements

Microanalyses (C, H, N) were performed in a Perkin-Elmer 240C elemental analyzer.

Mass spectra were recorded on a Perkin Elmer (USA) Flexer SQ 300 MS Mass

Spectrometer operating in ESI mode. Infrared spectra were measured with a Shimadzu

IR Affinity - 1 FT-IR spectrometer using KBr pellet. Electronic absorption spectra

were recorded on a Jasco V-570 UV/VIS/NIR spectrophotometer using a pair of

matched quartz cell of path length of 1 cm. Electron paramagnetic resonance spectra were recorded on a JEOL, Japan Model: JES - FA200 ESR spectrometer with X and Q band. Room temperature solution EPR spectra were recorded using an aqueous cell and frozen glass spectra were recorded in liquid nitrogen using a quartz dewer. Electrochemical measurements were done with the help of a Bioanalytical system CV-27 electrochemical analyzer and a BAS model X-Y recorder at 298K under dinitrogen. A standard three electrode cell consisting of a platinum working electrode, a platinum auxiliary electrode and a Ag/AgCl reference electrode was used. Tetrabutylammonium perchlorate ( $[N(n-Bu)_4]ClO_4$ ) was used as supporting electrolyte.

#### 4.5. X-ray crystallography

##### 4.5.1. $[CuL(o-phen)] \cdot 3.5H_2O$ (**1**) and $[CuL(Imz)]$ (**2**)

Blue crystals of complex **1** were obtained from the slow evaporation of a methanol-acetonitrile (1:1) solution of **1** at room temperature while green crystals for **2** were obtained from the slow evaporation of a methanol-acetonitrile (2:1) solution of **2** at room temperature. A blue crystal of **1** with approximate size of 0.35 × 0.25 × 0.20 mm or a green crystal of **2** with approximate size of 0.4 × 0.2 × 0.2 mm was mounted on a Bruker Axs Kappa Apex2 diffractometer equipped with graphite-monochromated  $[Mo K\alpha, \lambda = 0.71073 \text{ \AA}]$  radiation. The unit cell parameters (Table 3) were determined by the method of difference vectors using reflections scanned from three different zones of the reciprocal lattice. The intensity data were measured using  $\omega$  and  $\varphi$  scan with frame width of  $0.5^\circ$ . The frames integration and data reduction were performed using Bruker SAINT-Plus (Version 7.06a) software [24]. The multi-scan

absorption corrections were applied to the data using SADABS software. The crystal of **1** is indexed in monoclinic system with space group  $C 2/c$  and lattice parameters  $a = 21.070(3) \text{ \AA}$ ,  $b = 20.629(3) \text{ \AA}$ ,  $c = 14.1300(16) \text{ \AA}$ ,  $\alpha = 90^\circ$ ,  $\beta = 128.704(3)^\circ$ ,  $\gamma = 90^\circ$ . On the other hand, the crystal of **2** is indexed in orthorhombic system with space group 'P c a 2<sub>1</sub>' and lattice parameters  $a = 9.3659(6) \text{ \AA}$ ,  $b = 17.4585(11) \text{ \AA}$ ,  $c = 18.1049(13) \text{ \AA}$ ,  $\alpha = 90^\circ$ ,  $\beta = 90^\circ$ ,  $\gamma = 90^\circ$ .

SIR-92 program [25] was used for solving the structure. Structure was refined using SHELXL-2014 (Sheldrick, 2014) program [26]. Successive difference fourier map showed the positions of all hydrogen atoms. However, the hydrogen positions were geometrically fixed and refined through riding model. The full matrix structure refinement was carried out through minimization of the function  $\sum(w(F_o^2 - F_c^2))^2$ , where  $w = [(\sigma(F_o^2))^2 + (0.1406P)^2]^{-1}$  for **1** and  $w = [(\sigma(F_o^2))^2 + (0.0449P)^2 + 1.2789P]^{-1}$  for **2**, and  $P = (F_o^2 + 2F_c^2)/3$ ,  $F_o^2$  is the measured intensity (i.e., intensity observed) and  $F_c^2$  is the intensity calculated. The final residual factors were  $R = 0.06$  and  $wR = 0.2326$  for **1** and  $R = 0.05$  and  $wR = 0.1452$  for **2**, respectively. The largest difference map peak was  $0.605 \text{ e/\AA}^3$  for **1** and the largest difference map peak was  $1.193 \text{ e/\AA}^3$  for **2**.

**Table 3.** Crystal data and structure refinement for complexes **1** and **2**.

Empirical formula	$C_{25}H_{24}CuN_3O_{5.50}$	$C_{16}H_{13}CuN_3O_2$
Formula weight	518.01	342.83

Temperature	293(2) K	293(2) K
Wavelength	0.71073 Å	0.71073 Å
Crystal system	monoclinic	orthorhombic
Space group	'C 2/c'	'P c a 2 <sub>1</sub> '
Unit cell dimensions	a = 21.070(3) Å	a = 9.3659(6) Å
	b = 20.629(3) Å	b = 17.4585(11) Å
	c = 14.1300(16) Å	c = 18.1049(13) Å
	∠ = 90°	∠ = 90°
	∠ = 128.704(3)°	∠ = 90°
	∠ = 90°	∠ = 90°
Volume	4792.9(10) Å <sup>3</sup>	2960.4(3) Å <sup>3</sup>
Z	8	8
Density (calculated)	1.436 Mg/m <sup>3</sup>	1.538 Mg/m <sup>3</sup>
Absorption coefficient	0.955 mm <sup>-1</sup>	1.485 mm <sup>-1</sup>
F(000)	2144	1400
Crystal size	0.350 x 0.250 x 0.200 mm <sup>3</sup>	0.400 x 0.200 x 0.200 mm <sup>3</sup>
Theta range for data collection	1.749 to 24.974°	1.166 to 26.997°
Index ranges	-24 ≤ h ≤ 24, -24 ≤ k ≤ 24, -16 ≤ l ≤ 15	-
	11 ≤ h ≤ 11, -22 ≤ k ≤ 22,	-
	23 ≤ l ≤ 23	-
Reflections collected	29447	46020

Independent reflections	4207 [R(int) = 0.0860]	6456 [R(int) = 0.0639]
Completeness to theta	= 24.974° 99.8 %	= 25.242°
100 %		
Absorption correction	Semi-empirical from equivalents	Semi-empirical from equivalents
Max. and min. transmission	0.78 and 0.65	0.78 and 0.65
Refinement method	Full-matrix least-squares on F <sup>2</sup>	Full-matrix least-squares on F <sup>2</sup>
Data / restraints / parameters	4207 / 45 / 352	6456 / 76 / 398
Goodness-of-fit on F <sup>2</sup>	0.995	1.101
Final R indices [I > 2σ(I)]	R1 = 0.0646, wR2 = 0.1742	R1 = 0.0478, wR2 = 0.1150
R indices (all data)	R1 = 0.1366, wR2 = 0.2326	R1 = 0.0865, wR2 = 0.1452
Extinction coefficient	n/a	n/a
Largest diff. peak and hole	0.605 and -0.839 e.Å <sup>-3</sup>	1.193 and -0.683 e.Å <sup>-3</sup>

#### 4.6. Methods for biological activity

##### 4.6.1. DNA binding studies

Electronic spectra of the compounds **1** and **2** were recorded using a Jasco V-570 UV/VIS/NIR spectrophotometer with incremental amounts of calf thymus DNA (CT-DNA) in order to get the binding constant for these compounds. The titration experiments were performed by keeping the complex concentration constant and by varying the concentration of ct-DNA from 0 to 40  $\mu\text{M}$  in 10 mM Tris-HCl buffer (pH 7.54).

#### 4.6.2. Cytotoxicity studies

##### 4.6.2.1. Cell culture and treatment

The human lung cancer cell line A549, breast cancer cell line MCF7, normal human keratinocyte HaCaT cells and human lung embryonic L132 cells were purchased from NCCS Pune. These cell lines were cultured in T-25 mm NUNC cell culture flasks with DMEM high glucose medium with 10% Fetal Bovine Serum (GIBCO performance plus grade, US origin) that was supplemented with penicillin (100 units/ml), streptomycin (100  $\mu\text{g}/\text{ml}$ ) gentamycin 50 $\mu\text{g}/\text{mL}$  and amphotericin B (2.5  $\mu\text{g}/\text{ml}$ ) at 37°C (5% CO<sub>2</sub> and 95 % O<sub>2</sub>) in a CO<sub>2</sub> incubator. Then these cells were sub cultured after they had reached 70-80 % confluence by trypsinization and used for further experimental purpose.

##### 4.6.2.2. 3-(4,5-Dimethylthiazol-2-yl)-2,5-diphenyltetrazolium bromide (MTT) assay

To evaluate the cytotoxicity of compounds **1** and **2**, MTT assay was performed on the above mentioned cancer and normal cell lines. Cell viability was determined by the

reduction of yellow MTT into purple formazan product by the enzymatic activity of mitochondrial dehydrogenase in the live cells following the method of Mabley et al. [27]. The cells were plated on 96 well plates at a density of  $4 \times 10^4$  per well and treated with complexes **1** and **2** as described at varying concentrations (starting from  $0.25 \mu\text{M}$  to  $10 \mu\text{M}$ ) was added with DMEM culture medium containing 10% FCS. MTT assay was carried out in triplicates. The cells were examined after 24 h incubation under phase contrast microscope and observed the cells morphology and photographed using Leica systems. Then, the medium was removed and the cells were treated with  $0.5 \text{ mg/ml}$  of MTT (Thiazolyl Blue Tetrazolium Bromide salt) in 1X PBS ( $150 \mu\text{L/well}$ ) and incubated for 4 h in a  $\text{CO}_2$  incubator. After 4 h incubation with MTT solution, the solution was removed and blue colored formazan crystal was solubilized with  $200 \mu\text{L}$  DMSO. The absorbance was measured at  $570 \text{ nm}$  using BioRad ELISA plate reader. The cytotoxicity of the free Schiff base ligand N-salicylidene-*o*-aminophenol was also studied using the human lung cancer A549 cell line with different concentrations ( $2.5 \mu\text{M}$ ,  $5 \mu\text{M}$ ,  $7.5 \mu\text{M}$  and  $10 \mu\text{M}$ ) of the free ligand.

#### 4.6.2.3. Cellular morphology assessment. Acridine orange (AO)/ Propidium iodide (PI) dual staining

A549 cells and L132 cells that were plated in 6-well plates at a density of  $5 \times 10^4$  were allowed to grow at  $37^\circ\text{C}$  in a humidified  $\text{CO}_2$  incubator until they were 70–80% confluent. Then these cells were treated with different concentrations of complexes **1** and **2** ( $1$ ,  $2.5$  and  $5 \mu\text{M}$ ) for 24 h. The culture medium was aspirated from each well

and cells were gently rinsed with PBS twice at room temperature. Equal volumes of cells from control and metal complex treated were stained with 1  $\mu\text{g/mL}$  of acridine orange and propidium iodide and incubated in the dark for 30 min, then viewed with Leica fluorescence microscope.

### **Acknowledgements**

We thank the SAIF, IIT-Madras for XRD facilities; and SAIF, IIT-Bombay for recording EPR of the compounds **1-2** using JEOL, Japan Model: JES - FA200 ESR spectrometer. A.P.K. thanks Mr. Atanu Banerjee and Dr. Rupam Dinda, Department of Chemistry, National Institute of Technology, Rourkela, India for help with the ESI-MS results, and Ms. Angela Samanta and Dr. Angshuman Sarkar, Cell and Molecular Biology Research Laboratory, Department of Biological Sciences, BITS-Pilani K. K. Birla Goa Campus for help with the cytotoxicity assay of the free Schiff base ligand with the A549 cell line. M.K. and A.P.K. thank Mr. Srimanta Halder and Dr. P. Bhavana, Department of Chemistry, BITS-Pilani K. K. Birla Goa Campus for help with the electrochemical studies. P.T.M. thanks the SERB/DST, Govt. of India for a research Scheme EMR/2016/000745 and the INSA for the scheme SP/IHS/2016. We thank the reviewers for their constructive suggestions to improve this manuscript.

### **Appendix A. Supplementary material**

Crystallographic data for the structural analysis have been deposited with the Cambridge Crystallographic Data Centre, numbers are CCDC 1584059 for compound **1** and CCDC 1584060 for compound **2**, respectively. These data can be obtained free of charge via <http://www.ccdc.cam.ac.uk/conts/retrieving.html>, or from the Cambridge

Crystallographic Data Centre, 12 Union Road, Cambridge CB2 1EZ, UK; Fax: (+044) 1223-336-033; or E-mail: deposit@ccdc.cam.ac.uk. Fig. S1 and Fig S2. ESI-MS of compounds **1** and **2**. Fig. S3. Electronic spectrum of compound **1**. Fig.S4. Electronic spectrum of **2** in CH<sub>3</sub>OH at room temperature. Fig. S5. Plot of cell viability versus concentrations of the compounds **1** and **2**. Fig. S6. Cell viability for the human lung cancer A549 cell line without (control) and with 5 M, 7.5 M and 10 M of the free Schiff base ligand N-salicylidene-*o*-aminophenol after 24 h incubation time. Tables S1 and S2. Bond lengths and bond angles of compounds **1** and **2**, respectively. Table S3. Binding constants of **1**, **2** and some similar reported compounds. Table S4. Comparison of IC<sub>50</sub> values of **1** and **2** with some recently reported Cu(II) complexes. Table S5. Therapeutic index (TI = IC<sub>50</sub> in normal cell/ IC<sub>50</sub> in cancer cell) of **1** and **2**.

## References

- [1] (a) P. Nagababu, A.K. Barui, B. Thulasiram, C. Shobha Devi, S. Satyanarayana, C.R. Patra, B. Sreedhar, J. Med. Chem. 58 (2015) 5226–5241; (b) C. Santini, M. Pellei, V. Gandin, M. Porchia, F. Tisato, C. Marzano, Chem. Rev. 114 (2014) 815–862, and references therein; (c) G. Barone, A. Terenzi, A. Lauria, A. M. Almerico, J.M. Leal, N. Busto, B. García, Coord. Chem. Rev. 257 (2013) 2848-2862, and references therein; (d) F. Tisato, C. Marzano, M. Porchia, M. Pellei and C. Santini, Med. Res. Rev. 30 (2010) 708-749.
- [2] (a) R.C. Todd, S.J. Lippard, Metallomics, 1 (2009) 280–291, and references therein; (b) C.X. Zhang, S.J. Lippard, Currn. Opin. Chem. Biol. 7 (2003) 481-489; (c) Q. P. Dou, M. Smith David, G. Daniel Kenyon, A. Kazi, Prog. Cell. Cycle Res. 5

(2003) 441-446; (d) Y. Xiao, D. Chen, X. Zhang, Q. Cui, Y. Fan, C. Bi, Q.P. Dou, *Int. J. Oncol.* 37 (2010) 81-87; (2e) Z. Zhang, C. Bi, S. M. Schmitt, Y. Fan, L. Dong, J. Zuo, Q. P. Dou, *J. Biol. Inorg. Chem.* 17 (2012) 1257-1267.

[3] (a) M. Chauhan, K. Banerjee, F. Arjmand, *Inorg. Chem.* 46 (2007) 3072–3082; (b) S. Ramakrishnan, S., M. Palaniandavar, *J. Chem. Sci.* 117 (2005) 179–186; (c) J. Lu, Q. Sun, J.-L. Li, L. Jiang, W. Gu, X. Liu, Jin-Lei Tian, Shi-Ping Yan, *J. Inorg. Biochem.* 137 (2014) 46–56; (d) V. Rajendiran, R. Karthik, M. Palaniandavar, H. Stoeckli-Evans, V.S. Periasamy, M. A. Akbarsha, B.S. Srinag, H. Krishnamurthy, *Inorg. Chem.* 46 (2007) 8208-8221; (e) S. Ramakrishnan, V. Rajendiran, M. Palaniandavar, V.S. Periasamy, B.S. Srinag, H. Krishnamurthy, M.A. Akbarsha, *Inorg. Chem.*, 48 (2009) 1309-1322.

[4] (a) S.K. Mal, M. Mitra, G. Kaur, V.M. Manikandamathavan, M.S. Kiran, A. Roy Choudhury, B. Unni Nair, R. Ghosh, *RSC Adv.*, 4 (2014) 61337–61342; (b) R. Vijayalakhmi, M. Kanthimathi, R. Parthasarathi, B. U. Nair, *Bioorg. Med. Chem.*, 14 (2006) 3300-3306; (c) S. Rajalakshmi, M. S. Kiran, B. U. Nair, *Eur. J. Med. Chem.*, 80 (2014) 393-406; (d) S. Rajalakshmi, T. Weyhermüller, M. Dinesh, B. U. Nair, *J. Inorg. Biochem.*, 117 (2012) 48-59; (e) V.M. Manikandamathavan, B.U. Nair, *Eur. J. Med. Chem.* 68 (2013) 244-252; (f) S. Rajalakshmi, T. Weyhermüller, A.J. Freddy, H.R. Vasanthi, B.U. Nair, *Eur. J. Med. Chem.* 46 (2011) 608-617.

[5] (a) U. Basu, I. Khan, A. Hussain, P. Kondaiah, A. R. Chakravarty, *Angew. Chem., Int. Ed.*, 51 (2012) 2658-2661; (b) U. Basu, I. Khan, D. Koley, S. Saha, P. Kondaiah, A. R. Chakravarty, *J. Inorg. Biochem.*, 116 (2012) 77 – 87; (c) T. K. Goswami, S.

Gadadhar, M. Roy, M. Nethaji, A. A. Karande, A. R. Chakravarty, *Organometallics*, 31 (2012) 3010-3021; (d) T. K. Goswami, B. V. S. K. Chakravarthi, M. Roy, A. A. Karande, A. R. Chakravarty, *Inorg. Chem.*, 50 (2011) 8452-8464.

[6] (a) M. G. Walker, V. Gonzalez, E. Chekmeneva, J. A. Thomas, *Angew. Chem., Int. Ed.*, 51 (2012) 12107- 12110; (b) C. Fabbro, H. Ali-Boucetta, T. D. Ros, K. Kostarelos, A. Bianco and M. Prato, *Chem. Commun.*, 48 (2012) 3911- 3926; (c) N. J. Farrer, L. Salassa and P. J. Sadler, *Dalton Trans.*, (2009) 10690- 10701.

[7] (a) M. Devereux, D. O. Shea, A. Kellett, M. McCann, M. Walsh, D. Egan, C. Deegan, K. Kedziora, G. Rosair, H. Muller-Bunz, *J. Inorg. Biochem.*, 101 (2007) 881-892; (b) M. O'Connor, A. Kellett, M. McCann, G. Rosair, M. McNamara, O. Howe, B. S. Creaven, S. McClean, A. Foltyn-Arfa Kia, D. O'Shea, M. Devereux, *J. Med. Chem.*, 55 (2012) 1957-1968.

[8] S. Tardio, I. Basanetti, C. Bignardi, L. Elviri, M. Tegoni, C. Mucchino, O. Bussolati, R. Franchi-Gazzola, L. Marchio, *J. Am. Chem. Soc.*, 133 (2011) 6235-6242.

[9] (a) D. Dey, G. Kaur, A. Ranjani, L. Gayathri, P. Chakraborty, J. Adhikary, J. Pasan, D. Dhanasekaran, A.R. Choudhury, M. A. Akbarsha, N. Kole, B. Biswas, *Eur. J. Inorg. Chem.* (2014) 3350-3358; (b) P. Adak, B. Ghosh, A. Bauza, A. Frontera,

A. J. Blake, C. M. Corbella, C. Das-Mukhopadhyay, S. K. Chattopadhyay, RSC Adv. 6 (2016) 86851-86861; (c) R.A. Festa, D.J. Thiele, Curr. Biol. 21 (2011) 877-883.

[10] (a) A. Draksharapu, A.J. Boersma, M. Leising, A. Meetsma, W.R. Browne, Gerard Roelfes, Dalton Trans. 44 (2015) 3647-3655; (b) V.M. Manikandamathavan, T. Weyhermüller, R. P. Parameswari, M. Sathishkumar, V. Subramanian, B.U. Nair, Dalton Trans., 43 (2014) 13018–13031; (c) D.J. Arndt Jovin and T.M. Jovin, Methods Cell Biol., 30 (1989) 417-448.

[11] (a) J.G. Da Silva, A.A. Recio Despaigne, S.R.W. Louro, C.C. Bandeira, E.M. Souza-Fagundes, H. Beraldo, European J. of Med. Chem. 65 (2013) 415-426; (b) C. Marzano, M. Pellei, F. Tisato, C. Santini, Anti-Cancer Agents in Med. Chem. 9 (2009) 185-211, and references therein.

[12] A.D. Tiwari, A.K. Mishra, S.B. Mishra, B.B. Mamba, B. Maji, S. Bhattacharya, Spectrochim. Acta Part A 79 (2011) 1050-1056.

[13] (a) Cheng-Yong Zhou, J. Zhao, Yan-Bo Wu, Cai-Xia Yin, P. Yang, J. Inorg. Biochem. 101 (2007) 10-18; (b) J. Liu, T. Zhang, T. Lu, L. Qu, H. Zhou, Q. Zhang, L. Ji, J. Inorg. Biochem. 91 (2002) 269-276.

[14] (a) B.M. Zeglis, V.C. Pierre, J.K. Barton, Chem. Commun. 44 (2007) 4565-4579; (b) S.S. Bhat, A.A. Kumbhar, H. Heptullah, A.A. Khan, V.V. Gobre, S.P. Gejji, V.G. Puranik, Inorg. Chem. 50 (2011) 545-558.

[15] M.K. Koley, N. Duraipandy, M.S. Kiran, B. Varghese, P.T. Manoharan, A.P. Koley, Inorg. Chim. Acta 466 (2017) 538–550.

- [16] (a) M.K. Koley, Om P.Chouhan, S. Biswas, J. Fernandes, A. Banerjee, A. Chattopadhyay, B. Varghese, P.T. Manoharan, A.P. Koley, *Inorg. Chim. Acta* 456 (2017) 179–198; (b) M.K. Koley, S.C. Sivasubramanian, B. Varghese, P.T. Manoharan, A.P. Koley, *Inorg. Chim. Acta* 361 (2008) 1485–1495.
- [17] H. Yoko, A.W. Addison, *Inorg. Chem.* 16 (1977) 1341-1349.
- [18] L.J. Fruglia. *J. Appl. Cryst.*, 30 (1997) 565-566.
- [19] F. Gao, H. Chao, F. Zhou, Y.-X. Yuan, B. Peng, L.-N. Ji, *J. Inorg. Biochem.* 100 (2006) 1487-1494.
- [20] W. D. Wilson, L. Ratmeyer, M. Zhao, L. Streckowski, D. Boykin, *Biochemistry* 32 (1993) 4098-4104.
- [21] (a) K.M. Guckian, B.A. Schweitzer, R.X. Ren, C.J. Sheils, D.C. Tahmassebi, E.T. Kool, *J. Am. Chem. Soc.* 122 (2000) 2213-2222; (b) K.M. Guckian, T.R. Krugh, E.T. Kool, *J. Am. Chem. Soc.* 122 (2000) 6841-6847.
- [22] (a) D.D. Li, J.L. Tian, W. Gu, X. Liu, H.H. Zeng, S.P. Yan, *J. Inorg. Biochem.* 105 (2011) 894-901; (b) V.M. Manikandamathavan, V. Rajapandian, A.J. Freddy, T. Weyhermuller, V. Subramanian, B.U. Nair, *Eur. J. Med. Chem.* 57 (2012) 449-458.

[23] (a) D. Vercammen, G. Brouckaert, G. Denecker, M. Van de Craen, W. Declercq, W. Fiers, P. Vandenabeele, *J Exp Med.* 188 (1998) 919–930; (b) G. Majno, I. Joris, *Am. J. Pathology*, 146 (1995) 1-13; (c) S.L. Fink, B.T. Cookson, *Infect. Immun.* 73 (2005) 1907-1916; (d) D. Wallach, Tae-Bong Kang, C.P. Dillon, D.R. Green, *Science* 352 (2016) 51; (e) T. Zhang, A. Saghatelian, *Biochim. Biophys. Acta.* 1831 (2013) 1542-1554; (f) J.E. Chipuk, G.P. McStay, A. Bharti, T. Kuwana, C.J. Clarke, L.J. Siskind, L.M. Obeid, D.R. Green, *Cell* 148 (2012) 988–1000; (g) E. Hollville, S.J. Martin, *Cell* 148 (2012) 845-846; (h) M. Yamanea, S. Moriyaa, H. Kokubab, *Biochem. Biophys. Reports* 11 (2017) 174–181.

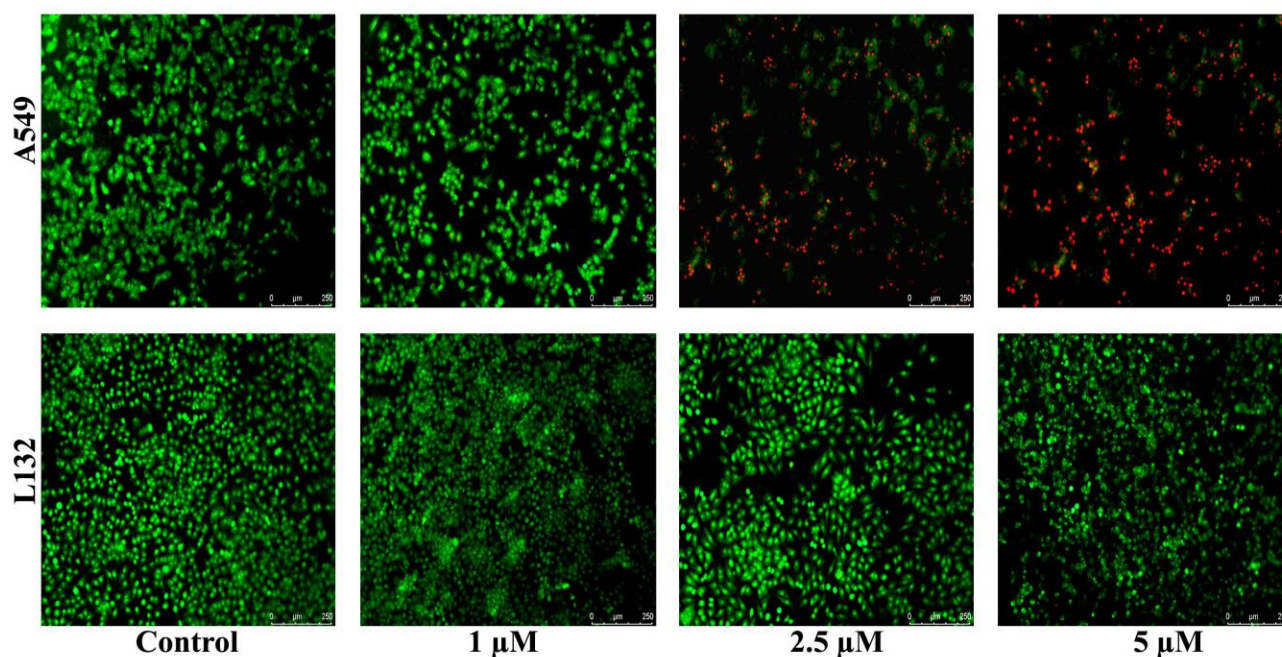
[24] Bruker-Nonius (2004). APEX-II and SAINT-Plus (Version 7.06a), Bruker AXS Inc., Madison, Wisconsin, USA.

[25] A. Altomare, G. Gasparano, C. Giacovazzo, A. Guagliardi. *J. Appl. Cryst.* 26 (1993) 343.

[26] (a) G.M. Sheldrick. (2012). SHELXL Version 2012. University of Göttingen, Germany; (b) G.M. Sheldrick. (2014). SHELXL Version 2014. University of Göttingen, Germany.

[27] J.G. Mabley, W.L. Suarez-Pinzon, G. Hasko, A.L. Salzman, A. Rabinovitch, E. Kun, C. Br. Szabo, *J. Pharmacol.* 133 (2001) 909-919.

## Graphical abstract



Two Cu(II) complexes containing the N-salicylidene-o-aminophenol ligand and 1,10-phenanthroline or imidazole as a coligand display remarkable cytotoxicity against the human lung cancer A549 cell line as well as the breast cancer MCF7 cell line as evident from the MTT assay. AO/PI dual staining assay for A549 cells suggests cell death via both apoptosis and necrosis for their anticancer activity.

## Highlights

Copper(II) complexes show intercalative DNA binding.

Show remarkable cytotoxicity for the lung cancer A549 cell line.

Also show significant cytotoxicity for the breast cancer MCF7 cell line.

Remarkably low toxic toward L132 human lung embryonic normal cell line.

In vitro AO/PI dual staining suggests cell death via both apoptosis and necrosis pathway for the anticancer activity.

## Figure Captions

**Scheme 1.** Synthesis of the ligand and the complexes.

**Fig. 1.** (A) ORTEP diagram of the compound **1** and (B) packing of the molecules in the unit cell. Bond lengths [ $\text{\AA}$ ] and angles [ $^\circ$ ] for **1**: N(1)-Cu(1) = 2.287(5); N(2)-Cu(1) = 2.016(5); N(3)-Cu(1) = 1.904(12); N(3')-Cu(1) = 1.981(17); O(1)-Cu(1) = 1.915(4); O(2)-Cu(1) = 1.933(4); N(3)-Cu(1)-O(1) = 100.8(5); N(3)-Cu(1)-O(2) = 78.2(5); O(1)-Cu(1)-O(2) = 162.51(18); O(1)-Cu(1)-N(3') = 76.5(6); O(2)-Cu(1)-N(3') = 101.9(6); N(3)-Cu(1)-N(2) = 167.6(4); O(1)-Cu(1)-N(2) = 91.41(17); O(2)-Cu(1)-N(2) = 90.85(19); N(3')-Cu(1)-N(2) = 167.2(6); N(3)-Cu(1)-N(1) = 97.7(3); O(1)-Cu(1)-N(1) = 100.14(16); O(2)-Cu(1)-N(1) = 97.29(17); N(3')-Cu(1)-N(1) = 100.0(4); N(2)-Cu(1)-N(1) = 77.79(18).

**Fig. 2.** (A) ORTEP diagram of the compound **2** and (B) packing of the molecules in the unit cell. Bond lengths [ $\text{\AA}$ ] and angles [ $^\circ$ ] for **2**: N(1)-Cu(1) = 1.943(11); N(2)-Cu(1) = 1.953(7); O(1)-Cu(1) = 1.927(6); O(2)-Cu(1) = 1.890(7); N(4)-Cu(2) = 1.926(9); N(5)-Cu(2) = 1.965(7), O(3)-Cu(2) = 1.932(6); O(4)-Cu(2) = 1.888(6); O(2)-Cu(1)-O(1) = 169.6(3); O(2)-Cu(1)-N(1) = 94.7(4); O(1)-Cu(1)-N(1) = 84.4(3); O(2)-Cu(1)-N(2) = 89.9(3); O(1)-Cu(1)-N(2) = 92.3(3); N(1)-Cu(1)-N(2) = 171.3(4).

**Fig. 3.** X-band EPR spectra of the compounds. (a)-(b) are RT spectra for **1-2** powder samples, (c)-(d)

are RT solution spectra for **1-2** in DMF, and (e)-(f) are LNT frozen glass spectra for **1-2** in DMF, respectively.

**Fig. 4.** (A) Change in electronic absorption spectra of **1** [ $2.5 \times 10^{-4}$  M] upon titration with CT-DNA (0–40  $\mu$ M) dissolved in 10 mM Tris–HCl buffer (pH 7.54). (B) Change in electronic absorption spectra of **2** [ $2.5 \times 10^{-4}$  M] upon titration with CT-DNA (0–25  $\mu$ M) dissolved in 10 mM Tris–HCl buffer (pH 7.54). Arrow shows the decrease in absorbance with respect to an increase in the concentration of CT-DNA. The figure in inset shows the linear fit of  $[\text{DNA}]/(\epsilon_a - \epsilon_f)$  versus  $[\text{DNA}]$ . The binding constant ( $K_b$ ) was calculated using the Eq. (1).

**Fig. 5.** Effect of increasing amount of complex **1** (red circles) and **2** (green squares) on the relative viscosity of CT-DNA (100  $\mu$ M) at room temperature in 10 mM Tris.HCl buffer (pH7.46).

**Fig. 6.** MTT assay for the compounds **1** and **2**. Panel A. A549 cell line, panel B. MCF7 cell line, panel C. L132 cell line, and panel D. HaCaT cell line.

**Fig. 7.** AO/PI staining results for compound **1** with A549 and L132 cell lines. Scale bar: 250  $\mu$ m.

**Fig. 8.** AO/PI staining results for compound **2** with A549 and L132 cell lines. Scale bar: 250  $\mu$ m.

**Fig. 9.** Cyclic voltammogram of the compounds ( $1.25 \times 10^{-3} \text{ mol L}^{-1}$ ) in DMF containing 0.1 M  $[\text{N}(\text{n-Bu})_4]\text{ClO}_4$  at a scan rate of  $100 \text{ mV s}^{-1}$ . Panels A and B for **1**, panels C and D for **2**, for initial negative and positive scans, respectively.

#### Appendix A. Supplementary material

*Manjuri K. Koley et al. Inorg. Chim. Acta*

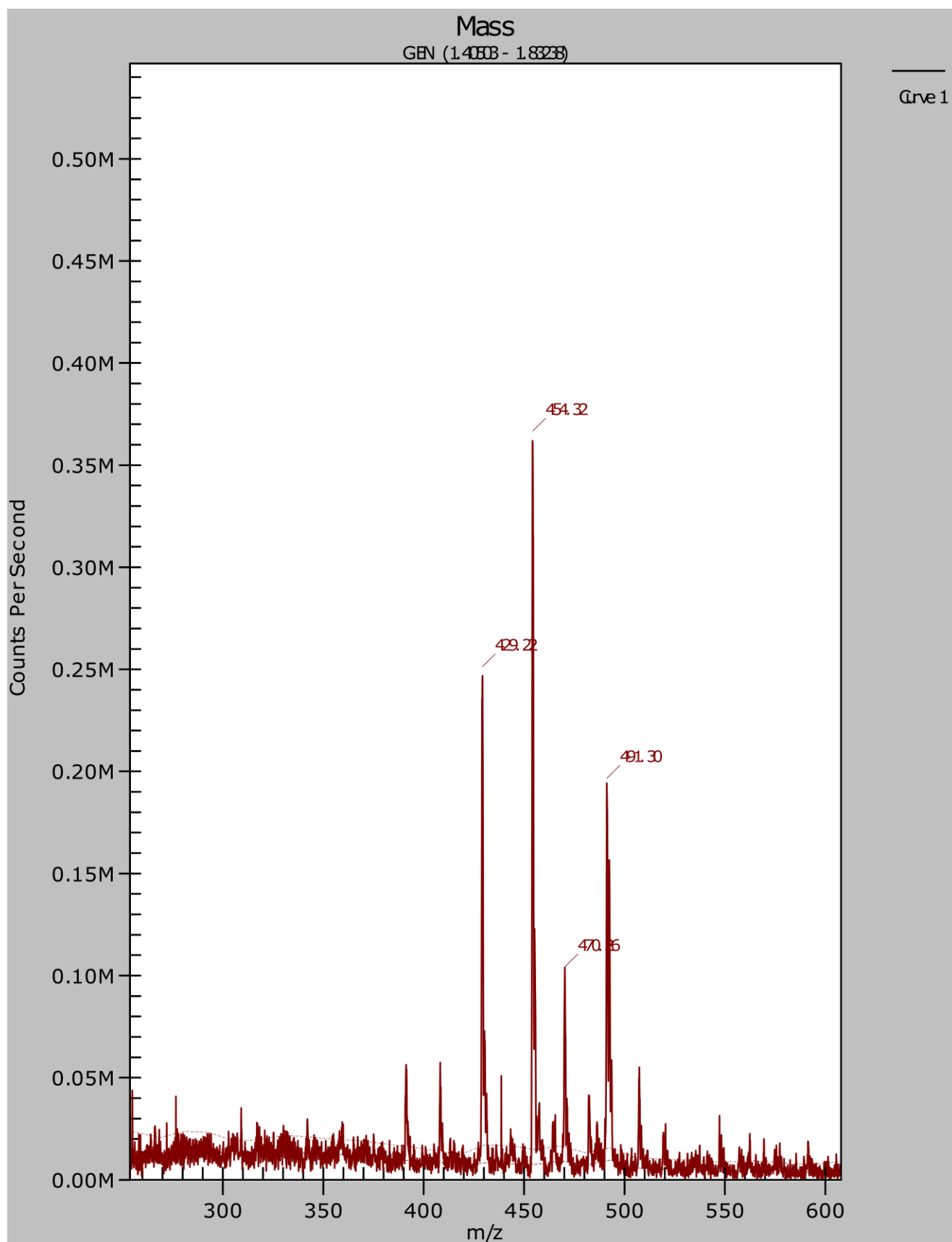


Fig. S1. ESI-MS:  $m/z$  454.30  $[M]^+$ , 491.30  $[(M+K)-2H]^+$ .

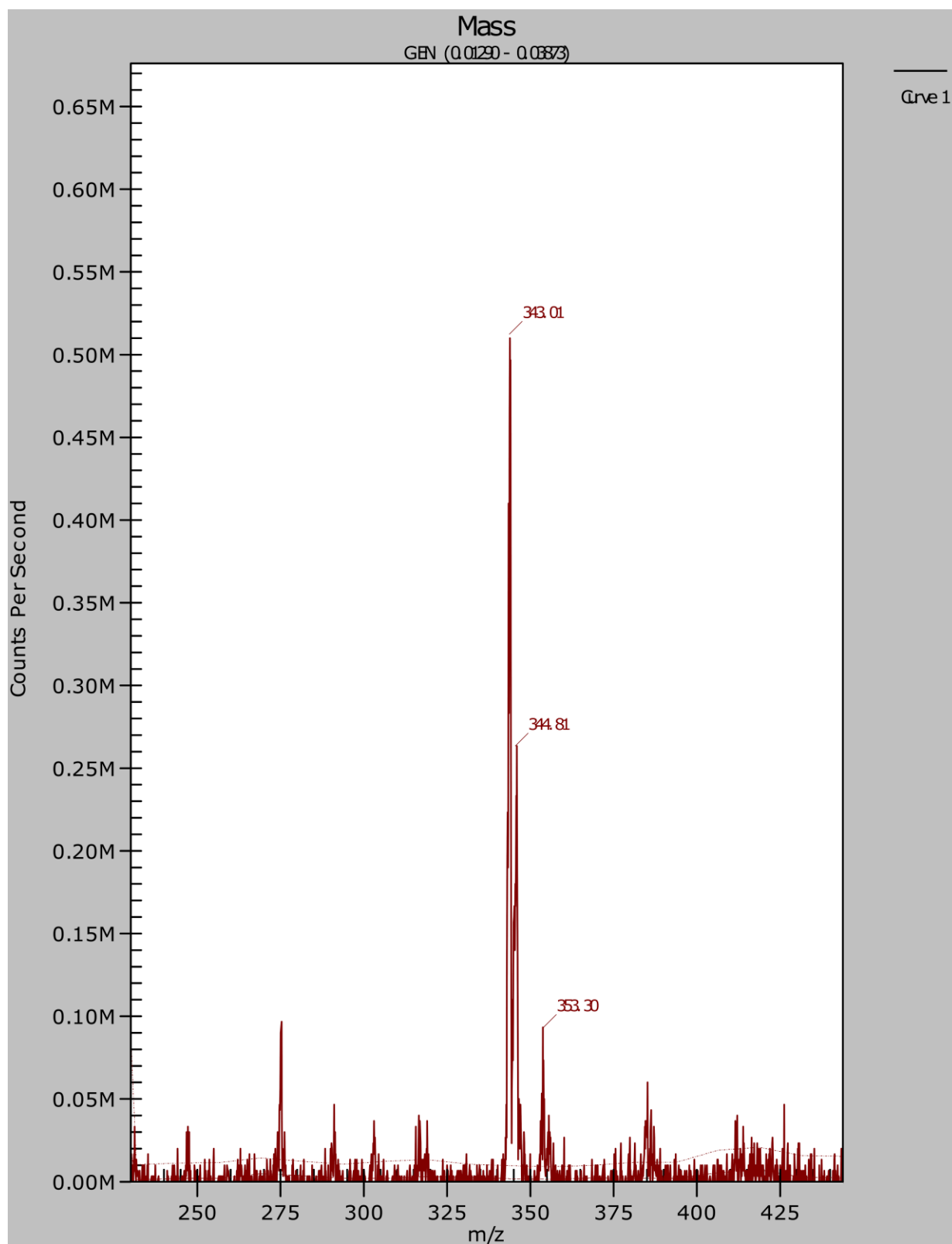


Fig. S2. ESI-MS:  $m/z$  343.01  $[M]^+$ , 344.81  $[M+2H]^+$ .

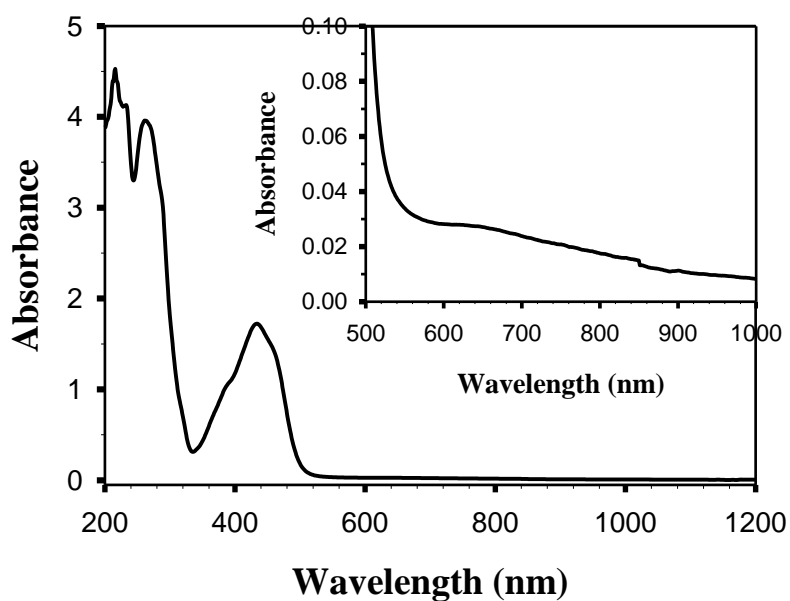


Fig.S3. Electronic spectrum of **1** [ $1.87 \times 10^{-4}$  M] in  $\text{CH}_3\text{CN}$  at room temperature.

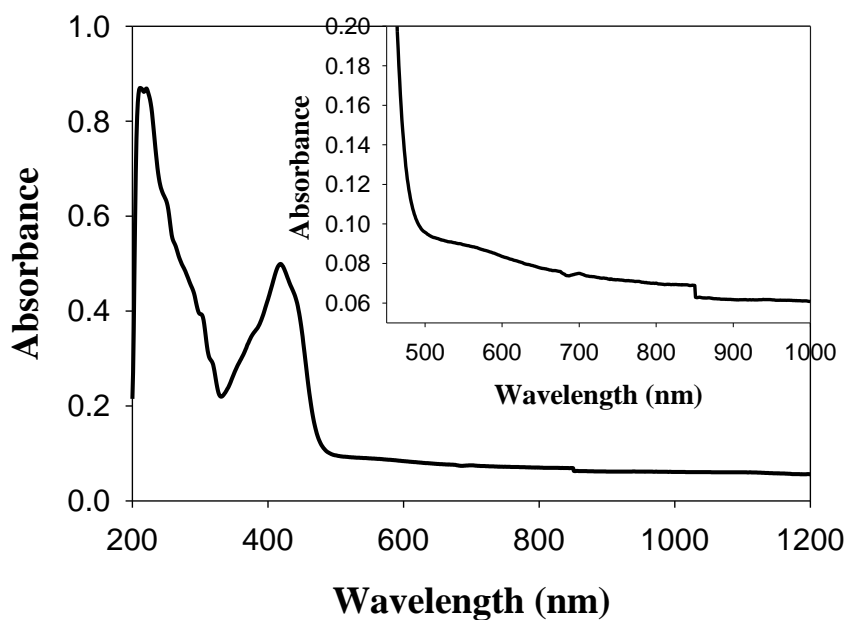


Fig.S4. Electronic spectrum of **2** [ $1.94 \times 10^{-3}$  M] in  $\text{CH}_3\text{OH}$  at room temperature.

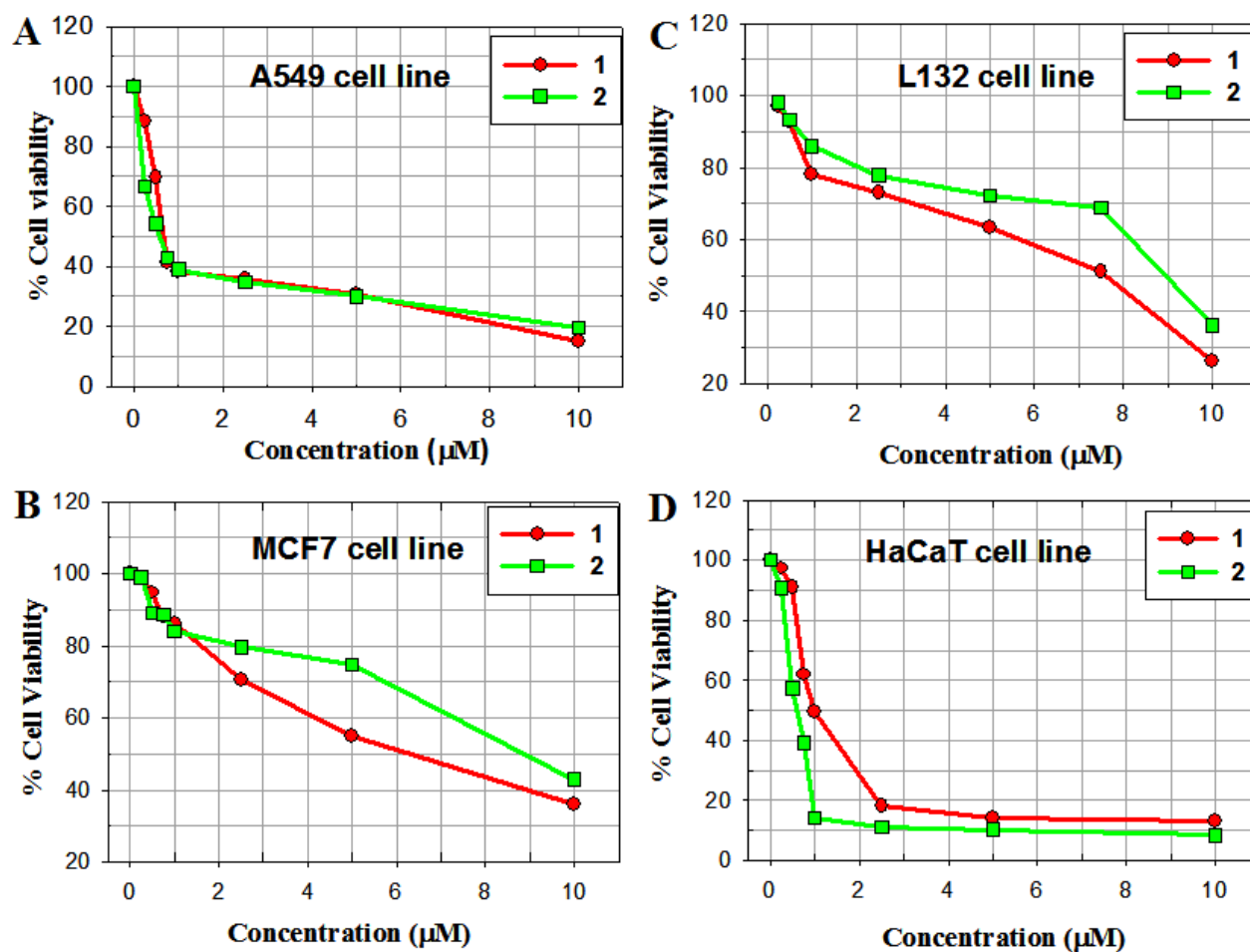


Fig. S5. Plot of cell viability versus concentrations of the compounds **1** and **2**: panel A. A549 cell line, panel B. MCF7 cell line, panel C. L132 cell line, and panel D. HaCaT cell line.

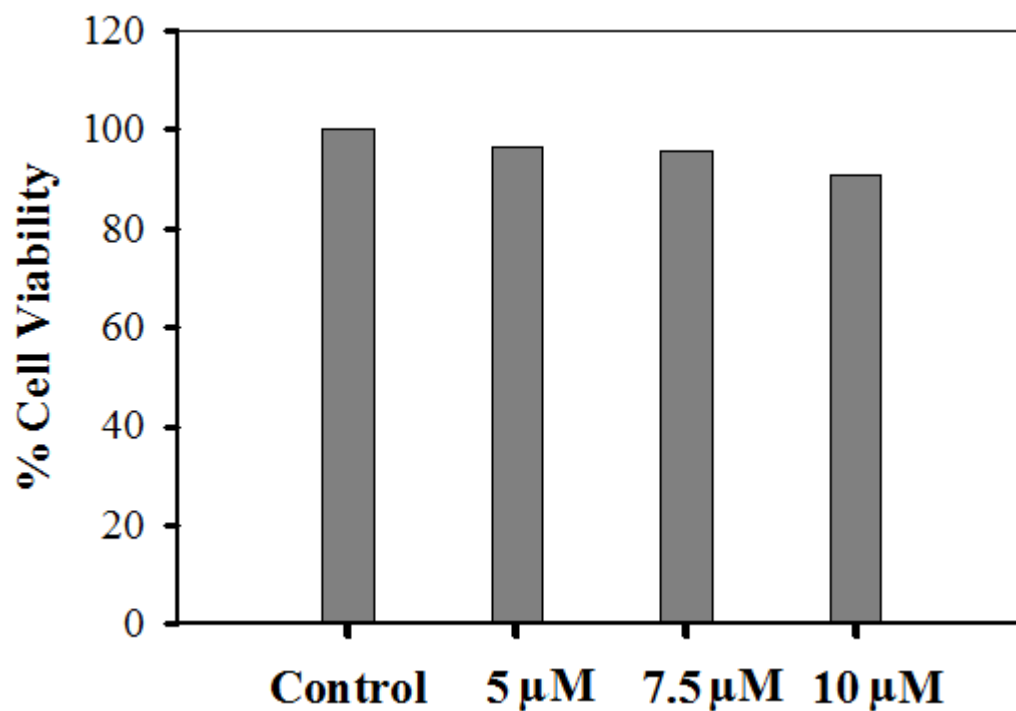


Fig. S6. Cell viability without (control) and with 5 M, 7.5 M, and 10 M of the free Schiff base ligand N-salicylidene-*o*-aminophenol for the human lung cancer A549 cell line after 24 h incubation time.

Table S1. Bond lengths [Å] and angles [°] for compound **1**.

---

C(1)-N(1)	1.319(7)
C(1)-C(2)	1.374(9)
C(1)-H(1)	0.9300
C(2)-C(3)	1.368(9)
C(2)-H(2)	0.9300

C(3)-C(4)	1.385(8)
C(3)-H(3)	0.9300
C(4)-C(12)	1.397(8)
C(4)-C(5)	1.416(9)
C(5)-C(6)	1.340(9)
C(5)-H(5)	0.9300
C(6)-C(7)	1.415(9)
C(6)-H(6)	0.9300
C(7)-C(11)	1.400(8)
C(7)-C(8)	1.413(8)
C(8)-C(9)	1.345(9)
C(8)-H(8)	0.9300
C(9)-C(10)	1.381(9)
C(9)-H(9)	0.9300
C(10)-N(2)	1.339(7)
C(10)-H(10)	0.9300
C(11)-N(2)	1.347(7)
C(11)-C(12)	1.458(8)
C(12)-N(1)	1.350(7)
C(13)-O(1)	1.311(7)
C(13)-C(14)	1.409(8)
C(13)-C(18)	1.420(9)
C(14)-C(15)	1.381(9)

C(14)-H(14)	0.9300
C(15)-C(16)	1.367(9)
C(15)-H(15)	0.9300
C(16)-C(17)	1.344(9)
C(16)-H(16)	0.9300
C(17)-C(18)	1.410(9)
C(17)-H(17)	0.9300
C(18)-C(19)	1.396(17)
C(18)-N(3')	1.548(18)
C(19)-N(3)	1.31(3)
C(19)-H(19)	0.9300
N(3)-C(20)	1.480(14)
N(3)-Cu(1)	1.904(12)
C(19')-N(3')	1.22(4)
C(19')-C(20)	1.46(2)
C(19')-H(19')	0.9300
N(3')-Cu(1)	1.981(17)
C(20)-C(25)	1.393(9)
C(20)-C(21)	1.408(10)
C(21)-C(22)	1.367(10)
C(21)-H(21)	0.9300
C(22)-C(23)	1.387(10)
C(22)-H(22)	0.9300

C(23)-C(24)	1.375(10)
C(23)-H(23)	0.9300
C(24)-C(25)	1.396(8)
C(24)-H(24)	0.9300
C(25)-O(2)	1.309(8)
N(1)-Cu(1)	2.287(5)
N(2)-Cu(1)	2.016(5)
O(1)-Cu(1)	1.915(4)
O(2)-Cu(1)	1.933(4)
O(3)-H(3A)	0.88(3)
O(3)-H(3B)	0.86(3)
N(1)-C(1)-C(2)	124.9(6)
N(1)-C(1)-H(1)	117.5
C(2)-C(1)-H(1)	117.5
C(3)-C(2)-C(1)	117.8(6)
C(3)-C(2)-H(2)	121.1
C(1)-C(2)-H(2)	121.1
C(2)-C(3)-C(4)	120.0(6)
C(2)-C(3)-H(3)	120.0
C(4)-C(3)-H(3)	120.0
C(3)-C(4)-C(12)	117.5(6)
C(3)-C(4)-C(5)	123.2(6)

C(12)-C(4)-C(5)	119.3(6)
C(6)-C(5)-C(4)	120.9(6)
C(6)-C(5)-H(5)	119.6
C(4)-C(5)-H(5)	119.6
C(5)-C(6)-C(7)	122.2(6)
C(5)-C(6)-H(6)	118.9
C(7)-C(6)-H(6)	118.9
C(11)-C(7)-C(8)	116.4(6)
C(11)-C(7)-C(6)	119.4(6)
C(8)-C(7)-C(6)	124.2(6)
C(9)-C(8)-C(7)	119.9(6)
C(9)-C(8)-H(8)	120.0
C(7)-C(8)-H(8)	120.0
C(8)-C(9)-C(10)	119.9(7)
C(8)-C(9)-H(9)	120.1
C(10)-C(9)-H(9)	120.1
N(2)-C(10)-C(9)	122.7(6)
N(2)-C(10)-H(10)	118.6
C(9)-C(10)-H(10)	118.6
N(2)-C(11)-C(7)	123.5(5)
N(2)-C(11)-C(12)	118.1(5)
C(7)-C(11)-C(12)	118.4(5)
N(1)-C(12)-C(4)	122.9(5)

N(1)-C(12)-C(11)	117.2(5)
C(4)-C(12)-C(11)	119.8(5)
O(1)-C(13)-C(14)	121.1(6)
O(1)-C(13)-C(18)	122.4(6)
C(14)-C(13)-C(18)	116.5(6)
C(15)-C(14)-C(13)	120.4(6)
C(15)-C(14)-H(14)	119.8
C(13)-C(14)-H(14)	119.8
C(16)-C(15)-C(14)	122.6(6)
C(16)-C(15)-H(15)	118.7
C(14)-C(15)-H(15)	118.7
C(17)-C(16)-C(15)	118.7(7)
C(17)-C(16)-H(16)	120.7
C(15)-C(16)-H(16)	120.7
C(16)-C(17)-C(18)	121.7(7)
C(16)-C(17)-H(17)	119.2
C(18)-C(17)-H(17)	119.2
C(19)-C(18)-C(17)	107.4(8)
C(19)-C(18)-C(13)	132.2(8)
C(17)-C(18)-C(13)	120.2(6)
C(17)-C(18)-N(3')	140.4(10)
C(13)-C(18)-N(3')	99.3(9)
N(3)-C(19)-C(18)	121.3(14)

N(3)-C(19)-H(19)	119.3
C(18)-C(19)-H(19)	119.3
C(19)-N(3)-C(20)	117.8(12)
C(19)-N(3)-Cu(1)	122.0(13)
C(20)-N(3)-Cu(1)	120.2(10)
N(3')-C(19')-C(20)	114.6(19)
N(3')-C(19')-H(19')	122.7
C(20)-C(19')-H(19')	122.7
C(19')-N(3')-C(18)	115.8(17)
C(19')-N(3')-Cu(1)	123.6(18)
C(18)-N(3')-Cu(1)	120.6(12)
C(25)-C(20)-C(21)	120.3(7)
C(25)-C(20)-C(19')	140.6(11)
C(21)-C(20)-C(19')	98.7(11)
C(25)-C(20)-N(3)	103.7(8)
C(21)-C(20)-N(3)	136.0(9)
C(22)-C(21)-C(20)	121.2(7)
C(22)-C(21)-H(21)	119.4
C(20)-C(21)-H(21)	119.4
C(21)-C(22)-C(23)	118.5(7)
C(21)-C(22)-H(22)	120.7
C(23)-C(22)-H(22)	120.7
C(24)-C(23)-C(22)	120.9(7)

C(24)-C(23)-H(23)	119.5
C(22)-C(23)-H(23)	119.5
C(23)-C(24)-C(25)	121.6(7)
C(23)-C(24)-H(24)	119.2
C(25)-C(24)-H(24)	119.2
O(2)-C(25)-C(20)	120.0(6)
O(2)-C(25)-C(24)	122.5(7)
C(20)-C(25)-C(24)	117.4(7)
C(1)-N(1)-C(12)	116.8(5)
C(1)-N(1)-Cu(1)	134.1(4)
C(12)-N(1)-Cu(1)	109.1(3)
C(10)-N(2)-C(11)	117.5(5)
C(10)-N(2)-Cu(1)	124.7(4)
C(11)-N(2)-Cu(1)	117.7(4)
C(13)-O(1)-Cu(1)	120.3(4)
C(25)-O(2)-Cu(1)	117.4(4)
N(3)-Cu(1)-O(1)	100.8(5)
N(3)-Cu(1)-O(2)	78.2(5)
O(1)-Cu(1)-O(2)	162.51(18)
O(1)-Cu(1)-N(3')	76.5(6)
O(2)-Cu(1)-N(3')	101.9(6)
N(3)-Cu(1)-N(2)	167.6(4)
O(1)-Cu(1)-N(2)	91.41(17)

O(2)-Cu(1)-N(2)	90.85(19)
N(3')-Cu(1)-N(2)	167.2(6)
N(3)-Cu(1)-N(1)	97.7(3)
O(1)-Cu(1)-N(1)	100.14(16)
O(2)-Cu(1)-N(1)	97.29(17)
N(3')-Cu(1)-N(1)	100.0(4)
N(2)-Cu(1)-N(1)	77.79(18)
H(3A)-O(3)-H(3B)	106(4)

---

Symmetry transformations used to generate equivalent atoms:

#1  $x, -y, z - 1/2$

Table S2. Bond lengths [ $\text{\AA}$ ] and angles [ $^\circ$ ] for compound **2**.

---

C(1)-O(1)	1.319(11)
C(1)-C(6)	1.386(13)
C(1)-C(2)	1.397(13)
C(2)-C(3)	1.363(13)
C(2)-H(2)	0.9300
C(3)-C(4)	1.381(14)
C(3)-H(3)	0.9300
C(4)-C(5)	1.360(14)
C(4)-H(4)	0.9300

C(5)-C(6)	1.369(12)
C(5)-H(5)	0.9300
C(6)-N(1)	1.443(15)
C(7)-N(1)	1.234(12)
C(7)-C(8)	1.418(17)
C(7)-H(7)	0.9300
C(8)-C(13)	1.401(16)
C(8)-C(9)	1.405(16)
C(9)-C(10)	1.342(18)
C(9)-H(9)	0.9300
C(10)-C(11)	1.356(18)
C(10)-H(10)	0.9300
C(11)-C(12)	1.357(17)
C(11)-H(11)	0.9300
C(12)-C(13)	1.405(16)
C(12)-H(12)	0.9300
C(13)-O(2)	1.296(14)
C(14)-N(2)	1.316(13)
C(14)-N(3)	1.327(16)
C(14)-H(14)	0.9300
C(15)-N(3)	1.340(14)
C(15)-C(16)	1.345(18)
C(15)-H(15)	0.9300

C(16)-N(2)	1.377(14)
C(16)-H(16)	0.9300
N(1)-Cu(1)	1.943(11)
N(2)-Cu(1)	1.953(7)
N(3)-H(3A)	0.8600
O(1)-Cu(1)	1.927(6)
O(2)-Cu(1)	1.890(7)
C(17)-O(3)	1.335(11)
C(17)-C(18)	1.380(15)
C(17)-C(22)	1.404(15)
C(18)-C(19)	1.380(15)
C(18)-H(18)	0.9300
C(19)-C(20)	1.376(18)
C(19)-H(19)	0.9300
C(20)-C(21)	1.397(17)
C(20)-H(20)	0.9300
C(21)-C(22)	1.359(13)
C(21)-H(21)	0.9300
C(22)-N(4)	1.414(14)
C(23)-N(4)	1.264(11)
C(23)-C(24)	1.441(17)
C(23)-H(23)	0.9300
C(24)-C(25)	1.399(16)

C(24)-C(29)	1.407(15)
C(25)-C(26)	1.377(19)
C(25)-H(25)	0.9300
C(26)-C(27)	1.376(18)
C(26)-H(26)	0.9300
C(27)-C(28)	1.362(19)
C(27)-H(27)	0.9300
C(28)-C(29)	1.390(16)
C(28)-H(28)	0.9300
C(29)-O(4)	1.301(13)
C(30)-N(6)	1.295(16)
C(30)-N(5)	1.301(13)
C(30)-H(30)	0.9300
C(31)-C(32)	1.320(18)
C(31)-N(6)	1.364(14)
C(31)-H(31)	0.9300
C(32)-N(5)	1.343(14)
C(32)-H(32)	0.9300
N(4)-Cu(2)	1.926(9)
N(5)-Cu(2)	1.965(7)
N(6)-H(6)	0.8600
O(3)-Cu(2)	1.932(6)
O(4)-Cu(2)	1.888(6)

O(1)-C(1)-C(6)	119.5(8)
O(1)-C(1)-C(2)	121.6(10)
C(6)-C(1)-C(2)	118.9(10)
C(3)-C(2)-C(1)	119.6(12)
C(3)-C(2)-H(2)	120.2
C(1)-C(2)-H(2)	120.2
C(2)-C(3)-C(4)	121.2(11)
C(2)-C(3)-H(3)	119.4
C(4)-C(3)-H(3)	119.4
C(5)-C(4)-C(3)	119.1(11)
C(5)-C(4)-H(4)	120.5
C(3)-C(4)-H(4)	120.5
C(4)-C(5)-C(6)	121.2(12)
C(4)-C(5)-H(5)	119.4
C(6)-C(5)-H(5)	119.4
C(5)-C(6)-C(1)	120.0(10)
C(5)-C(6)-N(1)	127.2(11)
C(1)-C(6)-N(1)	112.8(8)
N(1)-C(7)-C(8)	126.3(11)
N(1)-C(7)-H(7)	116.8
C(8)-C(7)-H(7)	116.8
C(13)-C(8)-C(9)	118.9(11)

C(13)-C(8)-C(7)	124.1(12)
C(9)-C(8)-C(7)	117.1(11)
C(10)-C(9)-C(8)	122.0(12)
C(10)-C(9)-H(9)	119.0
C(8)-C(9)-H(9)	119.0
C(9)-C(10)-C(11)	120.7(13)
C(9)-C(10)-H(10)	119.6
C(11)-C(10)-H(10)	119.6
C(10)-C(11)-C(12)	118.5(12)
C(10)-C(11)-H(11)	120.7
C(12)-C(11)-H(11)	120.7
C(11)-C(12)-C(13)	124.1(12)
C(11)-C(12)-H(12)	118.0
C(13)-C(12)-H(12)	118.0
O(2)-C(13)-C(8)	124.5(10)
O(2)-C(13)-C(12)	119.7(11)
C(8)-C(13)-C(12)	115.8(12)
N(2)-C(14)-N(3)	110.7(14)
N(2)-C(14)-H(14)	124.7
N(3)-C(14)-H(14)	124.7
N(3)-C(15)-C(16)	106.6(9)
N(3)-C(15)-H(15)	126.7
C(16)-C(15)-H(15)	126.7

C(15)-C(16)-N(2)	108.9(9)
C(15)-C(16)-H(16)	125.5
N(2)-C(16)-H(16)	125.5
C(7)-N(1)-C(6)	125.0(10)
C(7)-N(1)-Cu(1)	124.4(7)
C(6)-N(1)-Cu(1)	110.5(8)
C(14)-N(2)-C(16)	105.4(10)
C(14)-N(2)-Cu(1)	125.2(9)
C(16)-N(2)-Cu(1)	129.3(7)
C(14)-N(3)-C(15)	108.4(10)
C(14)-N(3)-H(3A)	125.8
C(15)-N(3)-H(3A)	125.8
C(1)-O(1)-Cu(1)	112.4(6)
C(13)-O(2)-Cu(1)	125.4(7)
O(2)-Cu(1)-O(1)	169.6(3)
O(2)-Cu(1)-N(1)	94.7(4)
O(1)-Cu(1)-N(1)	84.4(3)
O(2)-Cu(1)-N(2)	89.9(3)
O(1)-Cu(1)-N(2)	92.3(3)
N(1)-Cu(1)-N(2)	171.3(4)
O(3)-C(17)-C(18)	122.1(10)
O(3)-C(17)-C(22)	118.4(9)
C(18)-C(17)-C(22)	119.6(10)

C(19)-C(18)-C(17)	121.0(12)
C(19)-C(18)-H(18)	119.5
C(17)-C(18)-H(18)	119.5
C(20)-C(19)-C(18)	118.9(12)
C(20)-C(19)-H(19)	120.6
C(18)-C(19)-H(19)	120.6
C(19)-C(20)-C(21)	120.7(12)
C(19)-C(20)-H(20)	119.6
C(21)-C(20)-H(20)	119.6
C(22)-C(21)-C(20)	120.2(13)
C(22)-C(21)-H(21)	119.9
C(20)-C(21)-H(21)	119.9
C(21)-C(22)-C(17)	119.6(10)
C(21)-C(22)-N(4)	127.6(11)
C(17)-C(22)-N(4)	112.8(8)
N(4)-C(23)-C(24)	125.1(11)
N(4)-C(23)-H(23)	117.4
C(24)-C(23)-H(23)	117.4
C(25)-C(24)-C(29)	120.0(11)
C(25)-C(24)-C(23)	115.8(11)
C(29)-C(24)-C(23)	124.2(11)
C(26)-C(25)-C(24)	120.5(13)
C(26)-C(25)-H(25)	119.7

C(24)-C(25)-H(25)	119.7
C(27)-C(26)-C(25)	118.6(13)
C(27)-C(26)-H(26)	120.7
C(25)-C(26)-H(26)	120.7
C(28)-C(27)-C(26)	122.1(12)
C(28)-C(27)-H(27)	119.0
C(26)-C(27)-H(27)	119.0
C(27)-C(28)-C(29)	120.7(13)
C(27)-C(28)-H(28)	119.7
C(29)-C(28)-H(28)	119.7
O(4)-C(29)-C(28)	118.0(11)
O(4)-C(29)-C(24)	124.0(10)
C(28)-C(29)-C(24)	118.0(12)
N(6)-C(30)-N(5)	113.6(14)
N(6)-C(30)-H(30)	123.2
N(5)-C(30)-H(30)	123.2
C(32)-C(31)-N(6)	106.6(10)
C(32)-C(31)-H(31)	126.7
N(6)-C(31)-H(31)	126.7
C(31)-C(32)-N(5)	110.1(9)
C(31)-C(32)-H(32)	125.0
N(5)-C(32)-H(32)	125.0
C(23)-N(4)-C(22)	122.9(9)

C(23)-N(4)-Cu(2)	124.9(6)
C(22)-N(4)-Cu(2)	112.2(7)
C(30)-N(5)-C(32)	104.2(10)
C(30)-N(5)-Cu(2)	126.0(9)
C(32)-N(5)-Cu(2)	129.7(7)
C(30)-N(6)-C(31)	105.4(10)
C(30)-N(6)-H(6)	127.3
C(31)-N(6)-H(6)	127.3
C(17)-O(3)-Cu(2)	112.1(6)
C(29)-O(4)-Cu(2)	126.2(7)
O(4)-Cu(2)-N(4)	95.1(4)
O(4)-Cu(2)-O(3)	170.7(3)
N(4)-Cu(2)-O(3)	84.3(3)
O(4)-Cu(2)-N(5)	90.1(3)
N(4)-Cu(2)-N(5)	171.3(4)
O(3)-Cu(2)-N(5)	91.7(3)

---

Symmetry transformations used to generate equivalent atoms:

Table S3. Binding constants of **1**, **2** and some similar reported compounds.

Complex	$K_b$ ( $M^{-1}$ )	Ref.
<b>1</b>	$1.53 \times 10^5$	This work
<b>2</b>	$3.13 \times 10^5$	This work
[Cu(pabt)(OH <sub>2</sub> )]ClO <sub>4</sub>	$1.47 \times 10^5$	[16]
[Cu(pabt)(Imz)]ClO <sub>4</sub>	$2.03 \times 10^5$	[16]
[Cu(pabt)(N-MeImz)]ClO <sub>4</sub>	$2.09 \times 10^5$	[16]

Table S4. Comparison of IC<sub>50</sub> values of **1** and **2** with some recently reported Cu(II) complexes.

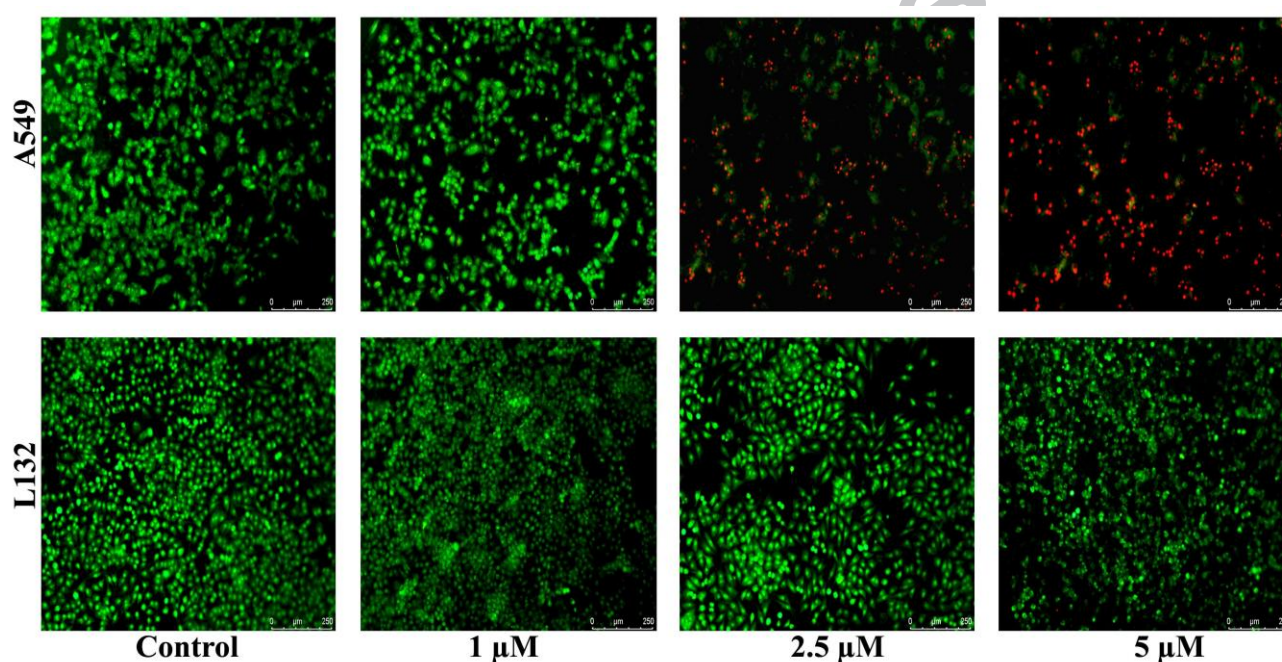
Complex [Ref.]	Type of complex	$K_b$ ( $M^{-1}$ )	IC <sub>50</sub> ( $\mu M$ )	
			A549	MCF7
<b>1</b> [This study]	Cu(II) with N-salicylidene- <i>o</i> -aminophenol and 1,10-phenanthroline or imidazole	$1.53 \times 10^5$	0.67	6.30
<b>2</b> [This study]		$3.13 \times 10^5$	0.59	8.88
[Cu( <i>o</i> -phen)HL] [Ref. 15]	Cu(II) containing carbohydrazone and 1,10-phenanthroline $H_3L = o$ - $HOC_6H_4C(H)=N NH C(OH)=N N=$	$1.18 \times 10^5$	0.44	2.70
[Cu( <i>o</i> -phen)LCu(OAc)] [Ref. 15]		$1.26 \times 10^5$	0.22	4.10
[Cu( <i>o</i> -phen)LCu(OAc)]		$2.53 \times 10^5$	4.80	3.60

[Ref. 15]	C(H) C <sub>6</sub> H <sub>4</sub> OH- <i>o</i> , <i>o</i> -phen = 1,10-phenanthroline			
[Cu(Tf-PIP) <sub>2</sub> (H <sub>2</sub> O)] (ClO <sub>4</sub> ) <sub>2</sub> [Ref. 1a]	Cu(II) polypyridyl complexes IP = imidazophenanthroline	3.1 10 <sup>3</sup>	1.5	
[Cu(PYIP) <sub>2</sub> (H <sub>2</sub> O)](ClO <sub>4</sub> ) <sub>2</sub> [Ref. 1a]		5.2 10 <sup>5</sup>	38.20	
[Cu(CN-PIP) <sub>2</sub> (H <sub>2</sub> O)] (ClO <sub>4</sub> ) <sub>2</sub> [Ref. 1a]		6.3 10 <sup>3</sup>	71.8	
[Cu(PIP) <sub>2</sub> (H <sub>2</sub> O)](ClO <sub>4</sub> ) <sub>2</sub> [Ref. 1a]		2.2 10 <sup>4</sup>	0.6	
[Cu(L)Cl](ClO <sub>4</sub> ) [Ref. 3c]	ternary Cu(II) complexes	3.57 10 <sup>5</sup>	0.9	0.46
[Cu(L)Br <sub>2</sub> ] [Ref. 3c]	L= (2-((quinolin-8-ylimino)methyl)pyridine))	3.45 10 <sup>6</sup>	0.43	0.46
[Cu(itpy)(NO <sub>3</sub> )(H <sub>2</sub> O)](NO <sub>3</sub> ) .2H <sub>2</sub> O [Ref. 4e]	Cu(II) imidazole terpyridine complexes (itpy = imidazole terpyridine)	Kb <sub>1</sub> = 4.23 10 <sup>4</sup> Kb <sub>2</sub> = 5.92 10 <sup>3</sup>	0.81 (GI <sub>50</sub> )	
[Cu(Itpy)(ClO <sub>4</sub> )(H <sub>2</sub> O)](ClO <sub>4</sub> ) [Ref. 4e]		Kb <sub>1</sub> = 2.01 10 <sup>4</sup> Kb <sub>2</sub> = 3.21 10 <sup>4</sup>	0.64 (GI <sub>50</sub> )	
[Cu(tpy)(Cl) <sub>2</sub> ] [Ref. 22b]	Cu(II)terpyridine complexes	not studied	37.5	

[Cu(tpy)(NO <sub>3</sub> ) <sub>2</sub> (H <sub>2</sub> O)] [Ref. 22b]	tpy = terpyridine ptpy = pyridine terpyridine	not studied	40.4	
[Cu(ptpy)Cl <sub>2</sub> ].H <sub>2</sub> O.HCl [Ref. 22b]		not studied	41.2	
[Cu(itpy)(dmp)](NO <sub>3</sub> ) <sub>2</sub> [Ref. 4f]	Cu(II) complexes with substituted terpyridine ligand	3.3 10 <sup>5</sup>	76	
[Cu(ptpy)(dmp)](NO <sub>3</sub> ) <sub>2</sub> [Ref. 4f]	(itpy = imidazole terpyridine, ptpy = pyridine terpyridine, dmp = dimethyl phenanthroline)	2.3 10 <sup>5</sup>	71	

Table S5. Therapeutic index (TI = IC<sub>50</sub> in normal cell/ IC<sub>50</sub> in cancer cell) of **1** and **2**.

Complex	L132		HaCaT	
	A549	MCF7	A549	MCF7
<b>1</b>	11.3	1.2	1.5	0.2
<b>2</b>	15.2	1.0	1.0	0.1

**Graphical abstract**

Two Cu(II) complexes containing the N-salicylidene-o-aminophenol ligand and 1,10-phenantroline or imidazole as a coligand display remarkable cytotoxicity against the human lung cancer A549 cell line as well as the breast cancer MCF7 cell line as evident from the MTT assay. AO/PI dual staining assay for A549 cells suggests cell death via both apoptosis and necrosis for their anticancer activity.

### Highlights

Copper(II) complexes show intercalative DNA binding.

Show remarkable cytotoxicity for the lung cancer A549 cell line.

Also show significant cytotoxicity for the breast cancer MCF7 cell line.

Remarkably low toxic toward L132 human lung embryonic normal cell line.

In vitro AO/PI dual staining suggests cell death via both apoptosis and necrosis pathway for the anticancer activity.

ACCEPTED MANUSCRIPT

**Table 1.** EPR parameters for compounds **1** and **2** derived from the spectra at RT and LNT.

Compound/state/temp.	$\nu$ (GHz)	g value	HFS values (mT)
<b>1-</b> DMF frozen glass at LNT	9.138	$g_{\parallel} = 2.21$ $g_{\perp} = 2.09$	$A_{\parallel} = 20.67$ $A_{\perp} < \text{linewidth}$
<b>1-</b> DMF solution at RT	9.434	$g = 2.11$ $\Delta_{pp} \approx 4.4$ to 3.9mT	$A_{\text{iso}} = 7.30$
<b>1-</b> Powder at RT	9.447	$g_{\parallel} = 2.14$ $g_{\perp} = 2.06$	Not resolved
<b>2-</b> DMF frozen glass at LNT	9.137	$g_{zz} = 2.21$ $g_{yy} \approx 2.09$ $g_{xx} = 1.97$	$A_{zz} = 19.99$ $A_{yy} \approx 7.0$ $A_{xx} < \text{linewidth}$
<b>2-</b> DMF solution at RT	9.433	$g = 2.085$ $\Delta_{pp} \approx 4.6$ to 4.13 mT	$A_{\text{iso}} = 8.50$
<b>2-</b> Powder at RT	9.448	$g_{11} = 2.11$ $g_{22} = 2.07$ $g_{33} = 2.05$	Not resolved

**Table 2.** IC<sub>50</sub> values for the compounds **1** and **2** calculated from the plot of cell viability versus concentration in the MTT assay.

Cell line	IC <sub>50</sub> (μM) for	
	Compd. <b>1</b>	Compd. <b>2</b>
A549	0.67	0.59
MCF 7	6.30	8.88
L132	7.60	8.95
HaCaT	0.99	0.60

**Table 3.** Crystal data and structure refinement for complexes **1** and **2**.

---

Empirical formula	$C_{25}H_{24}CuN_3O_{5.50}$	$C_{16}H_{13}CuN_3O_2$
Formula weight	518.01	342.83
Temperature	293(2) K	293(2) K
Wavelength	0.71073 Å	0.71073 Å
Crystal system	monoclinic	orthorhombic

Space group	'C 2/c'	'P c a 21'
Unit cell dimensions	a = 21.070(3) Å	a = 9.3659(6) Å
	b = 20.629(3) Å	b = 17.4585(11) Å
	c = 14.1300(16) Å	c = 18.1049(13) Å
	$\alpha = 90^\circ$	$\alpha = 90^\circ$
	$\beta = 128.704(3)^\circ$	$\beta = 90^\circ$
	$\gamma = 90^\circ$	$\gamma = 90^\circ$
Volume	4792.9(10) Å <sup>3</sup>	2960.4(3) Å <sup>3</sup>
Z	8	8
Density (calculated)	1.436 Mg/m <sup>3</sup>	1.538 Mg/m <sup>3</sup>
Absorption coefficient	0.955 mm <sup>-1</sup>	1.485 mm <sup>-1</sup>
F(000)	2144	1400
Crystal size	0.350 x 0.250 x 0.200 mm <sup>3</sup>	0.400 x 0.200 x 0.200 mm <sup>3</sup>
Theta range for data collection	1.749 to 24.974°	1.166 to 26.997°
Index ranges	-24 ≤ h ≤ 24, -24 ≤ k ≤ 24, -16 ≤ l ≤ 15 - 11 ≤ h ≤ 11, -22 ≤ k ≤ 22, 23 ≤ l ≤ 23	
Reflections collected	29447	46020
Independent reflections	4207 [R(int) = 0.0860]	6456 [R(int) = 0.0639]
Completeness to theta	= 24.974° 99.8 %	= 25.242° 100 %

Absorption correction	Semi-empirical from equivalents	Semi-empirical from equivalents
Max. and min. transmission	0.78 and 0.65	0.78 and 0.65
Refinement method	Full-matrix least-squares on F <sup>2</sup>	Full-matrix least-squares on F <sup>2</sup>
Data / restraints / parameters	4207 / 45 / 352	6456 / 76 / 398
Goodness-of-fit on F <sup>2</sup>	0.995	1.101
Final R indices [I > 2σ(I)]	R1 = 0.0646, wR2 = 0.1742	R1 = 0.0478, wR2 = 0.1150
R indices (all data)	R1 = 0.1366, wR2 = 0.2326	R1 = 0.0865, wR2 = 0.1452
Extinction coefficient	n/a	n/a
Largest diff. peak and hole	0.605 and -0.839 e.Å <sup>-3</sup>	1.193 and -0.683 e.Å <sup>-3</sup>

---

---